JOURNAL OF CHEMICAL PHYSICS VOLUME 113, NUMBER 15 15 OCTOBER 2000

State-to-state studies of ground state NH$(X\,^3\Sigma^-, v=0, J, N)$+Ne

Jan Leo Rinnenthal[a] and Karl-Heinz Gericke
*Institut für Physikalische und Theoretische Chemie, Technische Universität Braunschweig,
Hans-Sommer-Strasse 10, D-38106 Braunschweig, Germany*

(Received 6 June 2000; accepted 24 July 2000)

State-to-state rotational energy transfer of ground state NH$(X\,^3\Sigma^-, v=0, J, N)$ in collisions with Ne is examined. NH is exclusively generated in the metastable NH$(a\,^1\Delta)$ state via photodissociation of hydrazoic acid at a wavelength of 266 nm. The strongly forbidden NH$(a\,^1\Delta \rightarrow X\,^3\Sigma^-)$ intercombination transition around 794 nm is used to generate single state NH$(X\,^3\Sigma^-, v=0, J, N)$ applying the stimulated emission pumping technique. The ground state radicals are detected after a certain delay time with laser induced fluorescence (LIF) using the intense NH$(A\,^3\Pi \leftarrow X\,^3\Sigma^-)$ transition around 336 nm with respect to all quantum states. The collision induced energy flux between the different rotation and spin levels is studied in detail and a comprehensive set of state-to-state rate constants for inelastic collisions of NH$(X\,^3\Sigma^-, v=0, J, N)$ with Ne up to $N=7$ which include the effect of multiple collisions is given. The state-to-state rate constants are obtained by the use of an iterative integrated profiles method. We find a propensity for $(\Delta N=0,\ \Delta i=\pm 1)$ and $(\Delta N=\pm 1,\ \Delta i=0)$ transitions where N represents the quantum state for nuclear rotation and i represents the index of the spin component F_i. In most cases the energy transfer which changes the spin component and conserves the nuclear rotation quantum number N $(\Delta N=0,\ \Delta i=\pm 1)$, is the most effective energy transfer in collisions with Ne. The energy dependence of the transition efficiency concerning only the nuclear rotation quantum number N obeys an energy-gap law (EGL). © *2000 American Institute of Physics.* [S0021-9606(00)01139-9]

I. INTRODUCTION

The detailed knowledge of phenomena which occur when molecules or atoms collide with each other is essential for the qualitative and quantitative understanding of reactive and nonreactive processes occurring in nature. For example, in order to optimize combustion processes aiming at the minimization of the emission of pollutants it is necessary to know how the intermediates produced during a combustion process behave with respect to their quantum state populations which can differ from a thermal Boltzmann distribution. The most important processes in this respect are collision induced rotational energy transfer and vibration energy transfer. If a molecule collides (inelastic) with another molecule or an atom, then energy can be exchanged between the different degrees of freedom. A complete study of these energy transfer processes yields state-to-state rate constants for these collision induced transitions. The knowledge of these highly resolved rate constants allows to calculate the population distribution as a function of time for systems which are displaced from equilibrium. In interstellar space there are phenomena, for example, the existence of the OH maser radiation,[1,2] for which a detailed understanding of collision induced energy transfer processes is fruitful.[3] Also the NH radical can be found in interstellar space[4,5] and as an intermediate in combustion processes.[6,7] Theorists are interested in the results of collision experiments because the rate constants contain information about the shapes of the corresponding potential energy surfaces and their ongoing dynamics.

The progress of laser technology in the last decades has made it possible to develop efficient preparation and detection techniques which allow to perform state-to-state pump and probe experiments. Enormous experimental as well as theoretical work (calculations of potential energy surfaces with *ab initio* methods and calculations of the dynamics on potential energy surfaces) has been done so far. The improvement of *ab initio* methods and the increasing performance of modern computers make it possible nowadays that rate constants can be computed with good agreement with experimental determined values.

Already in the early 20th century the first qualitative studies of rotational energy transfer were performed.[8] Especially for collision induced rotational energy transfer numerous experiments were performed and a lot of experimental data is now available.[9–73] Most of the early experiments in the 70s were performed within an excited electronic state using the laser induced fluorescence (LIF) technique without time resolution.[13–27] The rate constants were usually calculated assuming that on the average only one collision occurs during the lifetime of the excited electronic state (single collision limit). Later, complete time resolution could be achieved by using the pump and probe technique for the study of rotational energy transfer in especially vibrationally excited levels within the electronic ground state, but also in excited electronic states.[49–58] First of all, molecules in the $^1\Sigma$, $^1\Pi$, $^2\Sigma$, and $^2\Pi$ electronic states were examined. For molecules in Π states one was interested in particular in the

---

[a] Electronic mail: j.rinnenthal@tu-bs.de

collision induced preference of the population of one of the two closely spaced Λ-sublevels.[1–3,60–73] However, studies on molecules in $^3\Sigma$ states where the coupling of the spin and the nuclear rotation is more complicated are still rare.[74–76,80]

Although our knowledge about the dynamics of collision induced rotational energy transfer in molecules has considerably grown, there is an essential lack of information at temperatures around several hundred Kelvin where a broad range of rotational states is populated but in terms of vibration most molecules are in the ground state. Although small radicals, like NH, populate the electronic and vibrational ground state for typical chemical temperatures up to about 1000 K there is no information available about state-to-state energy transfer from higher J states than $J=0,1$ within the $v=0$ manifold in the electronic ground state. The reason for this serious lack of information concerning state-to-state energy transfer is the problem of populating a single J state exclusively. Until now, state-to-state measurements of collision induced rotational energy transfer in the electronic and vibrational ground state have only been performed for the lowest rotational states ($J=0,1$). In these experiments the rotational temperature is decreased in a molecular beam. For instance, Dagdigian *et al.* performed such an experiment for the NH radical.[77] A further selection of different Λ levels and M_J substates can be achieved by the use of a hexapole electric field. This kind of experiments like this were performed by ter Meulen *et al.* for the OH radical.[78] Collision induced rotational energy transfer at higher rotational levels within the electronic ground state have only been performed for excited vibrational states ($v>0$)[79] whereas similar experiments for molecules in the vibrational ground state have only been performed for excited electronic states where one example is the NH molecule.[80–83] In summary, no state-to-state data are available for the most important chemical range of J states around several 100 K.

In the present work we present state-to-state rate constants for collision induced rotational energy transfer of a molecule in higher J levels within the electronic and vibrational ground state for the first time. We use a preparation technique which was already introduced in a previous publication.[84] This technique is based on two steps: In the first step the molecules are generated in a metastable excited state exclusively. In the second step (preparation) the electronic and vibrational ground state of the molecule is state selectively populated by stimulated emission pumping. In order to perform state-to-state studies of collision induced rotational energy transfer the previously prepared ground state molecules can be probed at different delay times by laser induced fluorescence (LIF) spectroscopy. The LIF spectra represent the population of all rotational states at different collision numbers. We use this preparation technique for the preparation of the $NH(X\,^3\Sigma^-,v=0,J,N)$ radical where a complete population inversion (100%) between the metastable $NH(a\,^1\Delta)$ state and the $NH(X\,^3\Sigma^-)$ state can be generated in the UV photolysis of hydrazoic acid at a wavelength of 266 nm[85–88] where the $NH(X\,^3\Sigma^-)+N_2$ channel is a spin forbidden process as illustrated in Fig. 1.

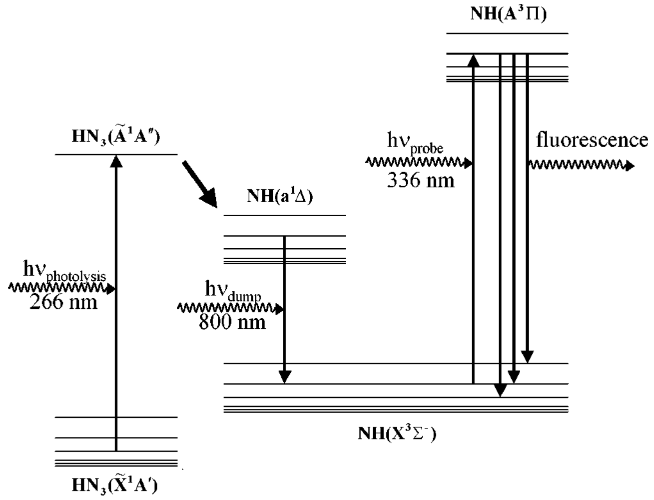

FIG. 1. Schematic picture of the three steps of the experiment [photolysis of HN_3, state-selective preparation of $NH(X\,^3\Sigma^-,v=0,J,N)$ radicals (dump) and detection of the $NH(X\,^3\Sigma^-,v=0,J,N)$ radicals with respect to all quantum states using laser induced fluorescence (LIF)].

II. EXPERIMENT

The general idea (Fig. 1) of the experiment is that in a first step a strong population inversion between the metastable excited $NH(a\,^1\Delta)$ state and the $NH(X\,^3\Sigma^-)$ state has to be generated. If this inversion is achieved $NH(X\,^3\Sigma^-,v=0,J,N)$ ground state radicals can be prepared in a second step state selectively with respect to all quantum states by stimulated emission pumping (dump) using the strongly forbidden ($\Delta S=1$, $\Delta L=2$) $NH(a\,^1\Delta\rightarrow X\,^3\Sigma^-)$ intercombination transition. The preparation of the $NH(X\,^3\Sigma^-,v=0,J,N)$ is completely state resolved with respect to the three spin components F_1, F_2, and F_3 which implies that also spin relaxation can be studied.

There are two processes which can destroy the necessary inversion. The radiative decay of $NH(a\,^1\Delta)$ and the effect of quenching. We determined the radiative lifetime τ of the free $NH(a\,^1\Delta)$ radical in a previous experiment to be $\tau\approx12.5$ s.[89] This value is much too high in order to destroy the inversion within a time period of 700 nanoseconds which is the time scale for the collision induced energy transfer at a typical total pressure of about 1 kPa in the observation chamber. Likewise, the quenching processes are not fast enough to destroy the inversion on the relevant time scale either. Typical quenching constants are listed in Table I. One recognizes that the rotational relaxation to be studied occurs clearly faster than the electronic quenching, the only exception being the quenching by the parent molecule HN_3. However, in

TABLE I. Quenching rate constants for the removal of $NH(a\,^1\Delta)$.

Collision partner	$k_q/10^{-11}\,cm^3\,s^{-1}$	Ref.
He	$<10^{-4}$	111
N_2	6.8×10^{-3}	111
O_2	6.2×10^{-3}	111
H_2	3.4×10^{-1}	111
HN_3	1.2×10^{1}	111
HF	7.3×10^{-2}	112

order to study NH–Ne collisions, the mixing ratio HN_3:Ne is set to 1:100 and at this mixing ratio the quenching by HN_3 is sufficiently low.

For the generation of the precursor of the NH radical, HN_3, we used two different methods. The generation can be performed by heating a mixture of sodium azide, NaN_3, and stearic acid under vacuum conditions. At about 85 °C HN_3 is the only evolving gas and can be stored in a glass bulb at a maximum pressure of about 1 kPa.[90] This method supplies HN_3 in excellent purity. Alternatively, HN_3 can be generated by adding dropwise small amounts of phosphoric acid under vacuum to NaN_3. This method is much simpler to handle and much faster but the generated HN_3 is less pure. It is polluted with phosphoric acid because of its vapor pressure and with water. However, test measurements showed that the purity of HN_3 generated by this method is sufficient for our purposes. The pressure in the glass bulb is monitored by a capacitance transducer (MKS Baratron 221AHS-D-100). In order to guarantee that NH–HN_3 collisions are rare in comparison to NH–Ne collisions and on one hand that the LIF signal is sufficient on the other hand, the stored HN_3 is diluted to a mixing ratio of $HN_3{:}Ne = 1{:}100$ at total pressures of 200 up to 2000 Pa in the observation chamber.

The vacuum system is realized by the use of an oil diffusion pump which reaches a base pressure of about 10^{-2} Pa. A second capacitance pressure transducer (MKS Baratron 221AHS-D-100) monitors the total pressure inside the observation chamber.

The experimental setup concerning lasers and electronics is shown in Fig. 2. All three lasers are aligned parallel to each other. The photolysis laser beam and the probe beam are focused by a 500 mm lens from one side into the observation chamber. The dump laser, which is counterpropagating the photolysis and the probe beams, is focused by a 300 mm lens because the transition probability of the NH($a\,^1\Delta \rightarrow X\,^3\Sigma^-$) intercombination transition is very low. The foci of the photolysis beam and the dump beam are most carefully overlapped in order to force as many NH($a\,^1\Delta$) radicals as possible into the $X\,^3\Sigma^-$ state. The focus of the probe laser beam ($f = 500$ mm) lies several cm beside the foci of both the photolysis and the dump laser beams. The detection laser beam surrounds the photolysis and the dump beams in their focal region. Thus, the detection efficiency of the expanding NH($X\,^3\Sigma^-$) cloud is maximized and the fly out of the NH($X\,^3\Sigma^-$) radicals out of the probe laser beam can be neglected. All laser beams are guided through baffles into the observation chamber in order to reduce the influence of scattered light.

The generation of NH($a\,^1\Delta$) (first step) is performed by a pulsed photodissociation of the parent molecule, HN_3, by a 266 nm light pulse of 30 mJ which is generated by the fourth harmonic of a Nd:YAG laser (Continuum Surelite II-10). At this wavelength NH is exclusively produced in its first excited electronic state, $a\,^1\Delta$. The nascent population distribution of the vibrational levels is known to be $(v=0){:}(v=1){:}(v=2)=(1){:}(0.3){:}(0.02)$.[91] The mean rotational energy of the nascent NH($a\,^1\Delta, v=0$) is 700 cm^{-1} whereas its kinetic energy is 7040 cm^{-1} what corresponds to a nascent velocity of 3320 m/s.[92] However, the relaxed velocity of a NH radical at a temperature of 300 K is about 700 m/s what is considerably lower. Therefore caution must be used for rotational relaxation studies because the translational motion of the NH radicals changes during the collisions that induce a change of the rotational quantum numbers (J,N). Since the scope of this work is the examination of collision induced rotational energy transfer in absence of translational relaxation, it must be guaranteed that the translational relaxation has already occurred before the ground state NH($X\,^3\Sigma^-, v=0, J, N$) radicals are prepared with the dump laser pulse. This can easily be achieved by choosing the delay time between the photolysis laser pulse and the dump laser pulse sufficiently long. However, if this delay time is chosen to be too long quenching of NH($a\,^1\Delta$) increases and influences the detection signal. Since the translational relaxation is about 10 times faster than the rotational relaxation to be studied, we use a delay time of 50 ns between the photolysis laser pulse and the dump laser pulse as the best compromise. This delay time is long enough for the relaxation of the translational motion of the NH radical which exhibits a similar mass like the atomic collision partner ($m_{NH}{:}m_{Ne} = 0.75$).

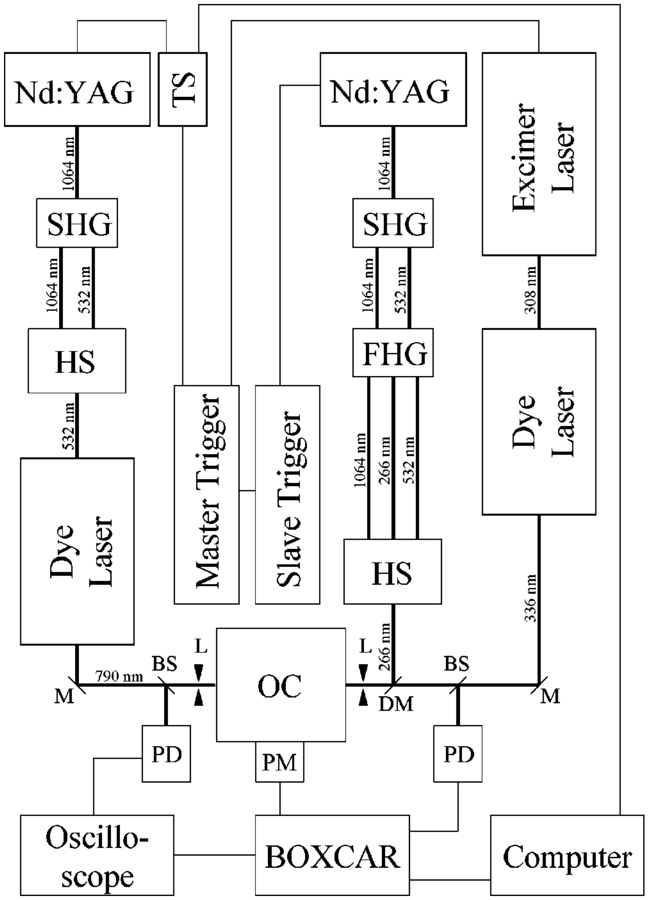

FIG. 2. Experimental setup. (TS=trigger suppressor, SHG=second harmonic generator, FHG=fourth harmonic generator, HS=harmonic separator, OC=observation chamber, M=mirror, DM=dichroitic mirror, BS=beam splitter, L=lens, MIC=microphone, PA=photoacoustic cell, PM=photomultiplier, PD=photodiode.)

The completely state-selective preparation of the NH($X\,^3\Sigma^-, v=0, J, N$) radicals (second step) is performed by stimulating the strongly forbidden intercombination tran-

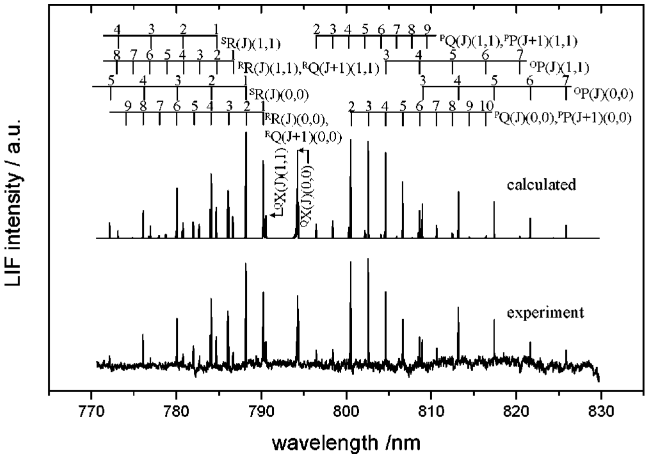

FIG. 3. Completely resolved spectrum of the strongly forbidden NH($a\,{}^1\Delta \rightarrow X\,{}^3\Sigma^-$) intercombination transition. The spectral resolution is 0.2 cm^{-1} (FWHM) and the rotational temperature is 300 K. All nine branches of the spectrum, ${}^{Q}P(J)$, ${}^{P}P(J)$, ${}^{Q}P(J)$, ${}^{P}Q(J)$, ${}^{Q}Q(J)$, ${}^{R}Q(J)$, ${}^{Q}R(J)$, ${}^{R}R(J)$, and ${}^{S}R(J)$, are assigned for the (0,0) and the (1,1) transitions. The spectrum is obtained by scanning the dump laser wavelength. For a comparison a calculated spectrum is also shown. The delay time between the photolysis laser pulse and the dump laser pulse was set to 100 ns whereas the delay time between the dump laser pulse and the detection laser pulse was set to 500 ns. The total pressure in the observation chamber was 10^4 Pa at a mixing ratio of Ne:HN$_3$=1×10^5.

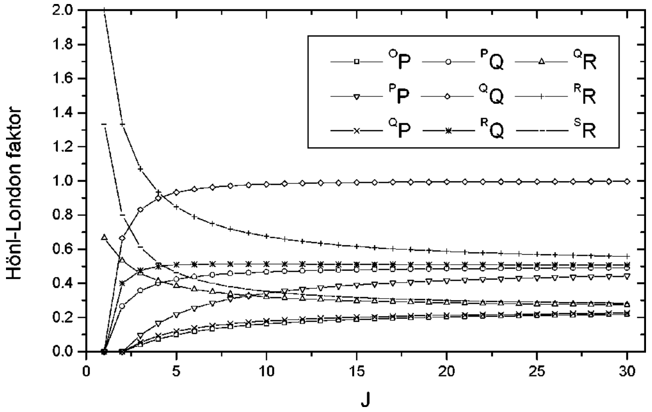

FIG. 4. Plot of the Hönl–London factors as a function of J.

sition NH($a\,{}^1\Delta \rightarrow X\,{}^3\Sigma^-$) which lies in the wavelength region from 770 to 830 nm. A Nd:YAG pumped dye laser (Continuum YG 680, TDL 60, IRP) with a pulse width of typically 7 ns supplies the desired wavelength of laser light with an energy of 30 mJ per pulse. The laser dyes LDS 765 (760–800 nm) and LDS 821 (795–840) are used with propylene carbonate and methanol as solvents.

The NH($a\,{}^1\Delta \rightarrow X\,{}^3\Sigma^-$) intercombination transition consists of nine branches which are denoted as ${}^{\Delta N}\Delta J(J)$. ΔN represents the change of the nuclear rotation quantum number N and ΔJ represents the change in the total angular momentum quantum number J. Thus, the nine branches are ${}^{O}P(J)$, ${}^{P}P(J)$, ${}^{Q}P(J)$, ${}^{P}Q(J)$, ${}^{Q}Q(J)$, ${}^{R}Q(J)$, ${}^{Q}R(J)$, ${}^{R}R(J)$, and ${}^{S}R(J)$.[89] Figure 3 shows the complete resolved spectrum of the NH($a\,{}^1\Delta \rightarrow X\,{}^3\Sigma^-$) intercombination transition. The branches are clearly separated by the change in the nuclear rotation quantum number ΔN (upper index). All branches of the ($v'=0$, $v''=0$) and ($v'=1$, $v''=1$) transitions are assigned. The S and the R branches are located on the left side, the Q branches are located in the middle of the spectrum and the P and O branches are located on the right-hand side of the spectrum. In a previous experiment we showed that at a pulse energy of 30 mJ the NH($a\,{}^1\Delta \rightarrow X\,{}^3\Sigma^-$) transition cannot be saturated completely.[89] Therefore, in order to prepare NH($X\,{}^3\Sigma^-,v=0,J,N$) radicals by stimulating the NH($a\,{}^1\Delta \rightarrow X\,{}^3\Sigma^-$) intercombination transition the Hönl-London factors[102] are necessary to calculate the efficiency of the preparation. Figure 4 represents a plot of the Hönl-London factors dependent on J. Not all branches are suitable for a preparation of NH($X\,{}^3\Sigma^-,v=0,J,N$). For instance, the branches ${}^{Q}P(J)$, ${}^{Q}Q(J)$, and ${}^{Q}R(J)$ are not completely separated with respect to their wavelength. Thus, a completely state selective preparation of NH($X\,{}^3\Sigma^-,v=0,J,N$) by using transitions of those branches is not possible. For the ${}^{O}P(J)$ branch the Hönl-London factors are too small, especially for low J values. Therefore, for the preparation of F_1 levels, NH($X\,{}^3\Sigma^-,v=0,J=N+1,N$), we used ${}^{R}Q(J)$ lines, for the preparation of the F_2 levels, NH($X\,{}^3\Sigma^-,v=0,J=N,N$), we used the ${}^{R}R(J)$ lines for low J values and the ${}^{P}P(J)$ lines for high J values. Finally, for the preparation of the F_3 levels, NH($X\,{}^3\Sigma^-,v=0,J=N-1,N$), we used the ${}^{P}Q(J)$ lines. It is not possible to prepare the level NH($X\,{}^3\Sigma^-,v=0,J=0,N=1$) because no transition is connected to that level. Also, the NH($X\,{}^3\Sigma^-,v=0,J=1,N=2$) level cannot be prepared state selectively. In fact, a transition for the preparation of that level exists, namely the ${}^{Q}R(1)$ line, but this line overlaps with the ${}^{Q}P(3)$ line what destroys the state selectivity. In total we prepared the following 16 levels:

$$
\begin{aligned}
F_1 \text{ levels:}\quad & (J=2,N=1),(J=3,N=2),(J=4,N=3),\\
& (J=5,N=4),\\
F_2 \text{ levels:}\quad & (J=1,N=1),(J=2,N=2),(J=3,N=3),\\
& (J=4,N=4),(J=5,N=5),\\
& (J=6,N=6),(J=7,N=7),\\
F_3 \text{ levels:}\quad & (J=2,N=3),(J=3,N=4),(J=4,N=5),\\
& (J=5,N=6),(J=6,N=7).
\end{aligned}
$$

In a third and last step the detection of the NH($X\,{}^3\Sigma^-,v=0,J,N$) radicals is performed after a certain delay time using the strong NH($A\,{}^3\Pi,v=0 \leftarrow X\,{}^3\Sigma^-,v=0$) transition [radiative lifetime τ=440±15 ns[106]] with respect to all quantum states. We recorded the spectra in the region 335.5–339 nm and used the branches $Q_2(J)$, ${}^{Q}P_{21}(J)$, ${}^{Q}R_{23}(J)$, ${}^{Q}P_{32}(J)$, $Q_3(J)$, ${}^{O}P_{12}(J)$, ${}^{O}Q_{13}(J)$, ${}^{O}P_{23}(J)$,

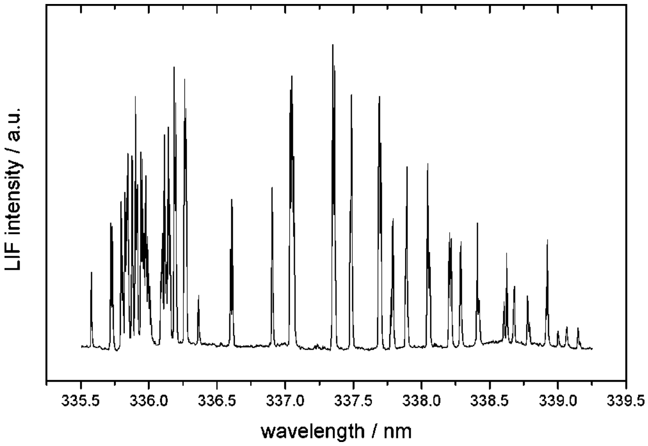

FIG. 5. Spectrum of the NH($A\,^3\Pi \leftarrow X\,^3\Sigma^-$) transition which was obtained by quenching of NH($a\,^1\Delta$). The delay time between the photolysis laser beam and the detection laser beam was set to 200 μs at a total pressure of 3 kPa in the observation chamber. The mixing ratio was HN_3:Ne$=1:100$.

$P_3(J)$, $^PQ_{23}(J)$, $P_2(J)$, $^PR_{13}(J)$, $P_1(J)$, $^PQ_{12}(J)$ for the population determination of the rotational levels. The desired wavelength region is supplied by an excimer laser (Radiant Dyes, RD-EXC-200) pumped dye laser (Lambda Physik, FL 3002) with a pulse energy of 2 mJ. The NH($A\,^3\Pi, v=0 \leftarrow X\,^3\Sigma^-, v=0$) spectra are recorded under saturated conditions which simplifies the population determination because the Hönl-London factors are equal to 1 and the line intensities only depend on the degeneracies of the two involved levels of a transition. The total fluorescence is monitored perpendicularly to all the laser beams through $f/1$ optics and an interference filter (330±30 nm). A boxcar integrator (Stanford Research System, DG 535) registers, amplifies and integrates the detected LIF signal. All lasers operate at a repetition rate of 10 Hz and are triggered via two coupled trigger generators, a master trigger generator (Stanford Research System DG 535) and a slave trigger generator (home built). The boxcar integrator is triggered by the probe laser beam via a photodiode. Finally, a computer records the experimental data for further processing.

In order to adjust the dump laser wavelength to a line of the NH($a\,^1\Delta \rightarrow X\,^3\Sigma^-$) transition that is suitable for the preparation of the desired NH($X\,^3\Sigma^-, v=0, J, N$) quantum state at least a weak LIF signal is necessary and therefore the probe laser beam has also to be adjusted to a suitable detection line of the NH($A\,^3\Pi \leftarrow X\,^3\Sigma^-, v=0, J, N$) transition. To adjust the detection laser beam to a suitable line the delay time between the photolysis laser beam and the probe laser beam is set to about 200 μs the dump laser is turned off and a total pressure of 3 kPa at a mixing ratio of HN_3:Ne $=1:100$ is used to induce the generation of NH($X\,^3\Sigma^-$) via quenching of NH($a\,^1\Delta$). By scanning the probe laser wavelength a completely relaxed spectrum of the NH($X\,^3\Sigma^-$) at 300 K can be recorded as shown in Fig. 5. When the detection laser is adjusted to a suitable line the total pressure in the observation chamber is set to 10^4 Pa at a mixing ratio of HN_3:Ne$=1:100000$. The time delay between the photolysis and the dump pulse is set to 100–150 ns whereas the time delay between the dump pulse and the detection pulse is set to 300–500 ns. These experimental parameters are optimal to record a spectrum of the NH($a\,^1\Delta \rightarrow X\,^3\Sigma^-$) transition by scanning the dump wavelength. A spectrum which was recorded that way is shown in Fig. 3. According to this procedure it is easy to adjust the dump laser wavelength to a line that is suitable for the preparation of the desired NH($X\,^3\Sigma^-, v=0, J, N$) quantum state in order to record NH($A\,^3\Pi \leftarrow X\,^3\Sigma^-$) detection spectra by scanning the probe laser wavelength which contain information about the collision induced rotational relaxation of the NH($X\,^3\Sigma^-, v=0, J, N$) radicals. The experimental parameters have to be changed again: The delay time between the photolysis laser beam and the dump laser beam is set to 50 ns whereas the time delay between the dump laser beam and the probe laser beam depends on the desired number of collisions and is usually set to 50–400 ns what is the most important time scale for the rotational relaxation phenomena at total pressures of 200–2000 Pa.

At these experimental conditions there are several lines within the wavelength region of the NH($A\,^3\Pi, v=0 \leftarrow X\,^3\Sigma^-, v=0$) detection spectrum that do not belong to that transition. These are, for instance, lines of the NH($A\,^3\Pi, v=1 \leftarrow X\,^3\Sigma^-, v=1$) transition. These lines appear mainly at higher delay times between the photolysis laser pulse and the probe laser pulse or at higher pressures. The reason for the appearance of these lines is the generation of NH($A\,^3\Pi, v=1$) via the quenching of NH($a\,^1\Delta$). In order to avoid these lines in the detection spectrum we subtracted the NH($A\,^3\Pi \leftarrow X\,^3\Sigma^-$) detection spectrum which is obtained when the dump laser pulse is suppressed from the detection spectrum which is obtained when the dump laser pulse is present. The resulting spectrum contains only information about the NH($X\,^3\Sigma^-, v=0$) radicals which have initially been prepared with the dump laser pulse. In the experiment the two spectra were recorded in two separated channels. In one channel we stored the spectrum with the dump laser pulse present whereas in the other channel we recorded the spectrum without the dump laser pulse. Every second pulse of the dump laser is suppressed by a trigger suppressor (see Fig. 2) that inhibits the Q switch of the dump laser system. In addition, the trigger suppressor generates a signal for the computer to indicate in which channel the LIF signal has to be stored. Figure 6 shows two screenshots of the oscilloscope (with and without the dump laser pulse) where the laser pulses, the LIF signal and the gate can be seen.

Using that technique we recorded for every initially prepared quantum state several NH($A\,^3\Pi, v=0 \leftarrow X\,^3\Sigma^-, v=0$) detection spectra at different pressures and delay times between the dump laser pulse and the probe laser pulse. From these spectra we extracted the population distributions. As an example, Fig. 7 shows three LIF spectra for three different total pressures in the observation chamber and the corresponding extracted population distributions.

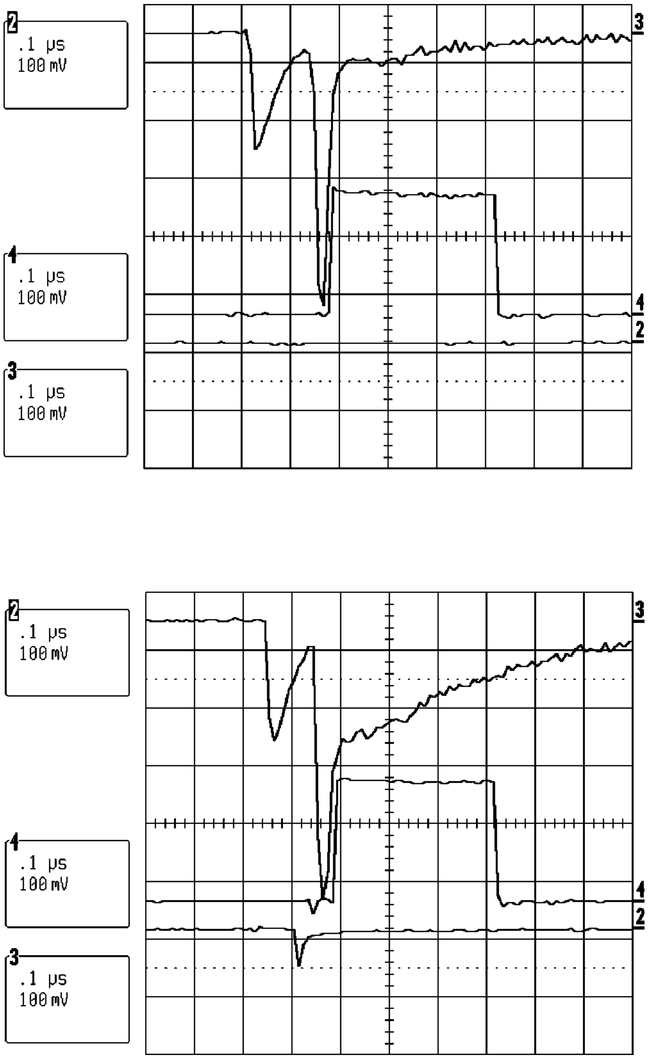

FIG. 6. Two screenshots of the oscilloscope which show the LIF signals which are obtained when the dump laser is suppressed by the trigger suppressor (above) and when the dump laser is present (below). Channel 2 shows the dump laser pulse when it is present, channel 3 shows the photolysis laser pulse, the detection laser pulse and the LIF signal. Finally, channel 4 shows the gate in which the LIF signal is integrated.

III. DATA ANALYSIS

A. Population determination

In order to determine the rate constants for collision induced transitions from the initial states NH($X\,^3\Sigma^-,v=0,J,N$) to the final states NH($X\,^3\Sigma^-,v=0,J',N'$) the time dependent population profiles $P^{J,N}_{J',N'}(t)$ have to be determined. The populations of NH($X\,^3\Sigma^-,v=0,J',N'$) are obtained from LIF spectra which are measured for several delay times. In order to extract the population data from the fluorescence spectra the line positions, i.e., the energies of the corresponding quantum states, and the line intensities (the transition probabilities) have to be known.

The NH LIF spectra which are used to extract the quantum state populations belong to the ($A\,^3\Pi\leftarrow X\,^3\Sigma^-$) electronic transition. This transition allows a population determination with respect to all quantum states. The NH($A\,^3\Pi\leftarrow X\,^3\Sigma^-$) transition is already examined since 1893 and was the subject of numerous investigations. A multitude of high accuracy experimental data is available today.[93–98]

The NH($A\,^3\Pi$) state is, especially for higher quantum numbers, close to coupling case (b), where coupling of the electronic spin with the internuclear axis is very weak. However, the electronic spin is coupled to N which represents the total angular momentum apart from spin. The rotational substates of the NH($A\,^3\Pi$) state are divided into the spin components $F_1\,(J=N+S=N+1)$, $F_2\,(J=N)$ and $F_3\,(J=N-S=N-1)$. The rotational levels in each spin component are Λ type doubled because of $\Lambda\neq 0$ (e/f levels). States with the parity $+(-1)^J$ are denoted as e states whereas states with the parity $-(-1)^J$ are denoted as f states.[99] Wave functions of $F_1(f)$, $F_2(e)$, and $F_3(f)$ states are symmetric concerning a reflection by a plane which contains the molecular axis (A' states) whereas wave functions of $F_1(e)$, $F_2(f)$, and $F_3(e)$ states are antisymmetric (A'' states).[100] The rotational substates of the NH($X\,^3\Sigma^-$) state are also divided into the three spin components $F_1\,(J=N+S=N+1)$, $F_2\,(J=N)$, and $F_3\,(J=N-S=N-1)$. However, in the case of NH($X\,^3\Sigma^-$) N is equal to the nuclear angular momentum because of $\Lambda=0$.

The electronic NH($A\,^3\Pi\leftarrow X\,^3\Sigma^-$) transition contain 27 branches (9 main branches and 18 satellite branches). Every branch represents a certain change of the total angular momentum quantum number J and the quantum number N. The different branches are denoted as $\Delta J_{i''}(J'')$ for the main branches and $^{\Delta N}\Delta J_{i',i''}(J'')$ for the satellite branches where $\Delta N=N'-N''$, $\Delta J=J'-J''$ and i indicates the spin component $F_i(i=N+2-J)$. Because of the fact that NH($A\,^3\Pi$) is close to case (b), which is valid even at low values of the angular momentum quantum number N, the following selection rules exist:[101]

$$\Delta J=J'-J''=-1,0,+1, \tag{1}$$

$$\Delta N=N'-N''=-1,0,+1 \quad \text{(only case b)}, \tag{2}$$

$$\Delta J=\Delta N \quad \text{(only case b)}, \tag{3}$$

$$-\leftrightarrow +. \tag{4}$$

If all selection rules are strictly valid there are only the 9 main branches. These are $^PP_{11}(J'')$, $^QQ_{11}(J'')$, $^RR_{11}(J'')$, $^PP_{22}(J'')$, $^QQ_{22}(J'')$, $^RR_{22}(J'')$, $^PP_{33}(J'')$, $^QQ_{33}(J'')$, $^RR_{33}(J'')$ which are usually denoted as $P_1(J'')$, $Q_1(J'')$, $R_1(J'')$, $P_2(J'')$, $Q_2(J'')$, $R_2(J'')$, $P_3(J'')$, $Q_3(J'')$, $R_3(J'')$. Since NH($A\,^3\Pi$) is only close to case (b) the selection rules (2) and (3) are not strictly valid which is the reason for the 18 satellite branches. The change in the angular momentum quantum number N by $-3,-2,-1,0,+1,+2,+3$ is represented by the letters N, O, P, Q, R, S, and T. Concerning J only P, Q, and R branches exist [selection rule (1)].

In order to calculate the LIF spectrum of the NH($A\,^3\Pi\leftarrow X\,^3\Sigma^-$) transition it is assumed that the lines are of Gaussian shape. The line shape of the detection laser line is assumed to be Gaussian as well. Thus, a detected line is represented by

$$I(\nu)=I_0 e^{-4\ln 2((\nu-\nu_0)/\Delta\nu)^2}, \tag{5}$$

where $\Delta\nu$ is the full line width at half maximum (FWHM).

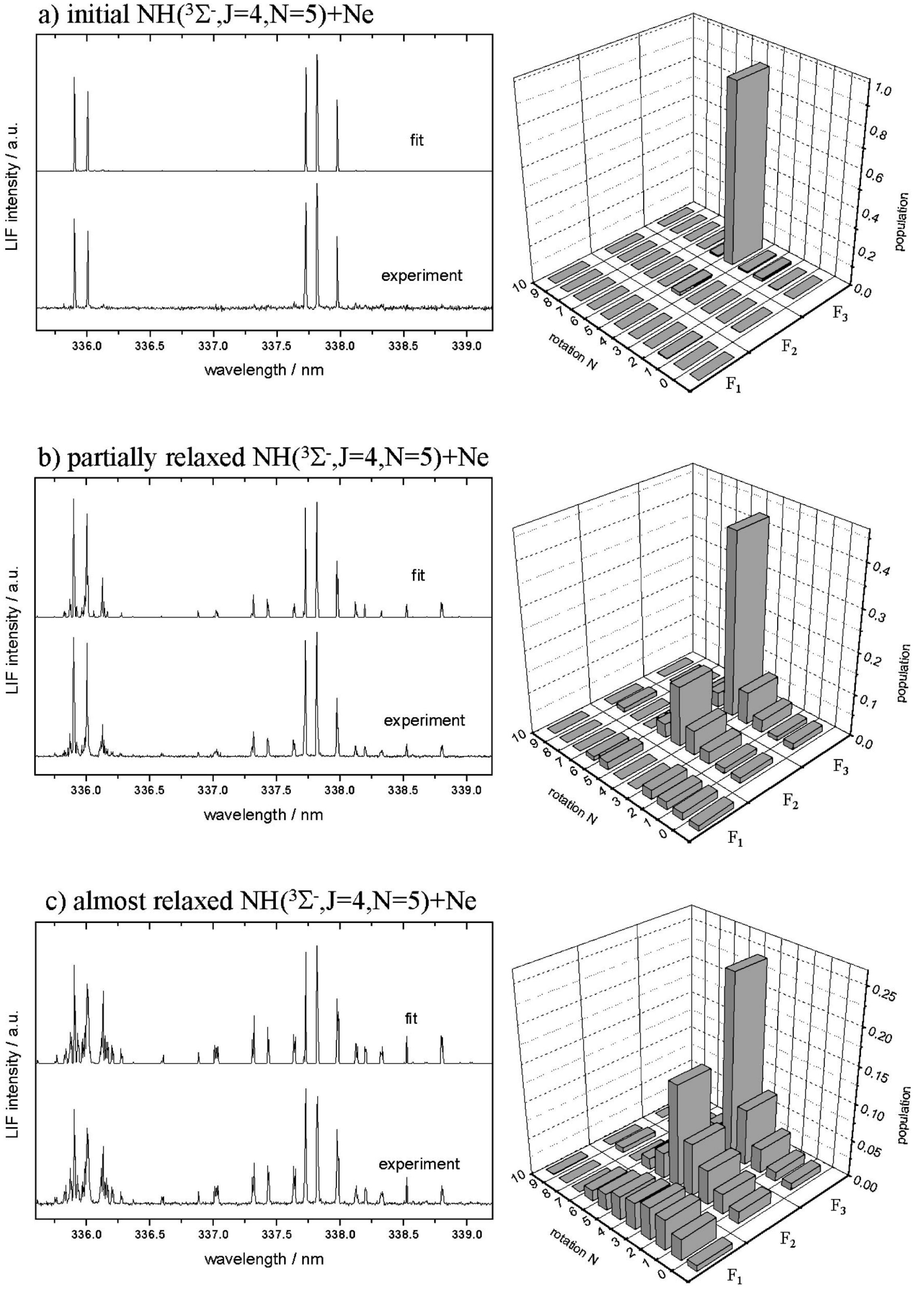

FIG. 7. Monitored and fitted NH($A\ ^3\Pi, v=0 \leftarrow X\ ^3\Sigma^-, v=0$) LIF spectra of NH($X\ ^3\Sigma^-, v=0$) which are obtained by scanning the detection laser (left) and the corresponding quantum state populations which are obtained by fitting the spectra (right). The initially prepared quantum state is NH($X\ ^3\Sigma^-, v=0, J=4, N=5$). The delay times between the photolysis laser pulse and the dump laser pulse and between the dump laser pulse and the detection laser pulse are both set to 50 ns. The mixing ratio is HN_3:Ne$=1:100$. The total pressure in the observation chamber in case (a) is 200 Pa what represents the nascent situation. Only NH($X\ ^3\Sigma^-, v=0, J=4, N=5$) radicals are present (all lines originate from the single $F_3(J=4, N=5)$ state). In case (b) the total pressure in the observation chamber is 1600 Pa. This represents the situation when the quantum state distribution is partly relaxed by collisions with Ne. In case (c) the total pressure in the observation chamber is 3200 Pa where the quantum state distribution is almost completely relaxed to a Boltzmann distribution at room temperature.

For the calculation of the line positions the energy levels of the rotational substates of NH($A\,^3\Pi$) and NH($X\,^3\Sigma^-$) are taken from Ref. 97. The wavelength of each line of the 27 branches is given by subtracting the energies of the two energy levels corresponding to a considered line. The intensity I_0 of a line is given by the expression

$$I_0=P(J',N')\cdot FC(v',v'')\cdot\frac{HL(J'',J')}{(2J''+1)},\tag{6}$$

where $P(J,N)$ is the population of the NH($X\,^3\Sigma^-,v=0,J,N$) state, FC(v',v'') is the Franck–Condon factor for a transition between v' (vibrational state of the upper electronic state $A\,^3\Pi$) and v'' (vibrational state of the lower electronic state $X\,^3\Sigma^-$) (in our case $v'=v''=0$) and HL(J'',J') is the Hönl-London factor of the transition. Expressions for the Hönl-London factors of the NH($A\,^3\Pi\leftarrow X\,^3\Sigma^-$) transition are given in Refs. 102–105. The Franck–Condon factor of the ($v'=0$, $v''=0$) transition is close to one.[106] If, like in our case, the detection laser is intense enough to saturate the transition, the line intensity factor HL(J'',J')/($2J''+1$) can be replaced by the factor

$$g_s=\frac{g(J')}{g(J'')+g(J')},\tag{7}$$

where $g(J')$ and $g(J'')$ are the degeneracies of the corresponding rotational substates of the NH($A\,^3\Pi$) and the NH($X\,^3\Sigma^-$) state.

From here on we use the following nomenclature: (J,N) represents a quantum state which initially has been prepared by the dump laser whereas (J',N') represents a quantum state which is populated by collision induced transitions out of the initially prepared quantum state (J,N). In order to determine the population distribution of NH($X\,^3\Sigma^-,v=0,J',N'$) at a certain delay time between the dump laser pulse and the detection laser pulse, the corresponding spectrum is fitted by first calculating a complete spectrum for some start values for the populations of the (J',N') states and then optimizing them iteratively while minimizing the least squares sum of the calculated and the measured spectrum. This is done for all measured spectra. Finally, the obtained population profiles $P^{J,N}_{J',N'}(t)$ for each (J',N') state are modeled using smoothing spline functions.

B. Solving the master equation

An ensemble of NH ground state radicals which has been prepared at time t_0 by a dump laser pulse in a single NH($X\,^3\Sigma^-,v=0,J,N$) state evolves in time obeying a system of coupled differential equations (master equation) of first order which can be written as

$$\begin{aligned}\frac{dP^{J,N}_{J,N}(t)}{dt}=[\mathrm{Ne}]\Bigg(&\sum_{(J',N')\neq(J,N)}^{(J',N')_{\max}}P^{J,N}_{J',N'}(t)k_{\mathrm{Ne}}^{(J,N)\leftarrow(J',N')}\\&-P^{J,N}_{J,N}(t)\sum_{(J',N')\neq(J,N)}^{(J',N')_{\max}}k_{\mathrm{Ne}}^{(J,N)\to(J',N')}\Bigg)\\&+[\mathrm{HN}_3]\Bigg(\sum_{(J',N')\neq(J,N)}^{(J',N')_{\max}}P^{J,N}_{J',N'}(t)k_{\mathrm{HN}_3}^{(J,N)\leftarrow(J',N')}\\&-P^{J,N}_{J,N}(t)\sum_{(J',N')\neq(J,N)}^{(J',N')}k_{\mathrm{HN}_3}^{(J,N)\to(J',N')}\Bigg)\end{aligned}\tag{8}$$

for each single level (here for the initially populated one). $P^{J,N}_{J,N}(t)$ is the population of the (J,N) state (lower index) at time t for an initial preparation of the same state (upper index). $P^{J,N}_{J',N'}(t)$ is the population of the (J',N') state at time t for an initial preparation of the (J,N) state. $k_{\mathrm{Ne}}^{(J,N)\leftarrow(J',N')}$ is the rate constant for a transition from the (J',N') state to the (J,N) state which is caused by a collision with Ne and $k_{\mathrm{Ne}}^{(J,N)\to(J',N')}$ vice versa. $k_{\mathrm{HN}_3}^{(J,N)\leftarrow(J',N')}$ and $k_{\mathrm{HN}_3}^{(J,N)\to(J',N')}$ are the rate constants for HN_3 as collision partner. [Ne] is the concentration of the collision partner Ne whereas $[HN_3]$ is the concentration of HN_3, the precursor of NH. The sums go over all states unequal to the prepared state. The first term in one of the two brackets describes the increase of the population of the (J,N) state by transitions from the neighboring (J',N') states whereas the second term describes the depopulation of the (J,N) state, respectively. The coupling of the equations is caused by the $P^{J,N}_{J',N'}(t)$. In order to predict the time dependent populations of all states $P^{J,N}_{J',N'}(t)$ considered, it is necessary to solve the master equation for given start conditions. These start conditions are the populations of each single state at time t_0, $P^{J,N}_{J',N'}(t_0)$, which are fixed with a pulse of the dump laser in the experiment. Because the preparation of a single NH($X\,^3\Sigma^-,v=0,J,N$) state with a dump laser pulse is completely state selective we obtain the well-defined start conditions:

$$P^{J,N}_{J',N'}(t_0)=\delta_{(J,N),(J',N')},\tag{9}$$

where $\delta_{(J,N),(J',N')}=1$ if $(J,N)=(J',N')$ and $\delta_{(J,N),(J',N')}=0$ if $(J,N)\neq(J',N')$.

For a solution of the master equation (8) the rate constants $k_{\mathrm{Ne}}^{(J,N)\leftarrow(J',N')}$, $k_{\mathrm{Ne}}^{(J,N)\to(J',N')}$, $k_{\mathrm{HN}_3}^{(J,N)\leftarrow(J',N')}$, and $k_{\mathrm{HN}_3}^{(J,N)\to(J',N')}$ are needed. In the following the extraction of the rate constants from the experimental data is described.

In order to minimize the influence of HN_3 on the relaxation process to be studied, HN_3 is diluted in the experiment to an appropriate mixing ratio of HN_3:Ne=100. This justifies the assumption $[HN_3]\to0$ which simplifies Eq. (8) dramatically assuming that only one collision partner, Ne, is present. Therefore, we write in the following $k_{\mathrm{Ne}}^{(J,N)\leftarrow(J',N')} = k^{(J,N)\leftarrow(J',N')}$, $k_{\mathrm{Ne}}^{(J,N)\rightarrow(J',N')} = k^{(J,N)\rightarrow(J',N')}$, $[\mathrm{Ne}]=[\mathrm{C}]$ (where C stands for collision partner) and obtain

$$\frac{dP^{J,N}_{J,N}(t)}{dt}=[\mathrm{C}]\left(\sum_{(J',N')\neq(J,N)}^{(J',N')_{\max}} P^{J,N}_{J',N'}(t)k^{(J,N)\leftarrow(J',N')} - P^{J,N}_{J,N}(t)\sum_{(J',N')\neq(J,N)}^{(J',N')_{\max}} k^{(J,N)\rightarrow(J',N')}\right). \tag{10}$$

At time t_0 when the dump laser prepares the initial state (J,N) we have the special situation $P^{J,N}_{J,N}(t_0)=1$ and $P^{J,N}_{J',N'}(t_0)=0$. This simplifies Eq. (10) in the $t\approx t_0$ regime as follows:

$$\lim_{t\rightarrow t_0}\frac{dP^{J,N}_{J,N}(t)}{dt}=-\sum_{(J',N')\neq(J,N)}^{(J',N')_{\max}}\frac{dP^{J,N}_{J',N'}(t_0)}{dt} = -\sum_{(J',N')\neq(J,N)}^{(J',N')_{\max}}[\mathrm{C}]k^{(J,N)\rightarrow(J',N')}. \tag{11}$$

Therefore, the rate constants can easily been written as

$$k^{(J,N)\rightarrow(J',N')}=\frac{1}{[\mathrm{C}]}\,\frac{dP^{J,N}_{J',N'}(t_0)}{dt} \tag{12}$$

which represents an approximation only valid in the $t\approx t_0$ regime (and also at low pressures) where $dP^{J,N}_{J',N'}(t_0)/dt$ is linear in t and only single collisions are considered.

However, reliable measurements at these conditions are difficult to realize because the populations of the states which are not initially populated, the (J',N') states, are very low in the $t\approx t_0$ and low pressure regime. But low populations cannot be measured with high accuracy because of the statistical noise of the spectra from which they are extracted. Therefore, much more information can be extracted if the experimental data are fitted not only slightly above $t\approx t_0$ (single collision regime) but also in the $t>t_0$ regime where multiple collisions have to be considered.

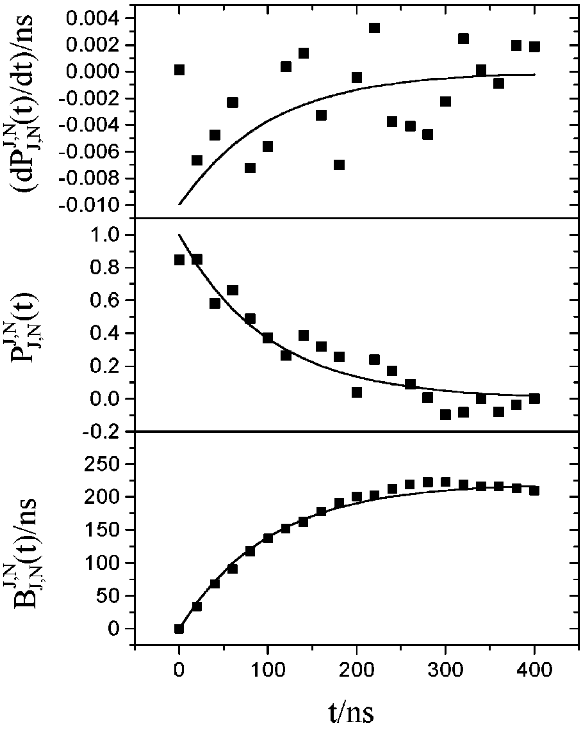

FIG. 8. Illustration of the effect of statistical noise of the experimental data on the profile $P^{J,N}_{J,N}(t)$ of a NH($X\,^3\Sigma^-,v=0,J,N$) state which has been prepared at time t_0 by a dump laser pulse (middle part of the picture), the integrated profile $B^{J,N}_{J,N}(t)$ (below) and the time derivation of the profile $dP^{J,N}_{J,N}(t)/dt$ (above). The squares in the middle of the picture represent typical experimental data of the time profile $P^{J,N}_{J,N}(t)$, on the other hand, the line graph in the middle of the picture represents the same data without any statistical moise. One can recognize that the time derivation of the experimental data of $P^{J,N}_{J,N}(t)$, $dP^{J,N}_{J,N}(t)/dt$ (squares above), exhibits an amplified statistical noise relative to the qualitative behavior of the noiseless curve (line graph above). However, the time integration of the experimental data $P^{J,N}_{J,N}(t)$, $B^{J,N}_{J,N}(t)$ (squares below), results in a reduced statistical noise relative to the qualitative behavior of the noiseless curve (line graph below). This shows that in order to fit the rate constants, $k^{(J,N)\rightarrow(J',N')}$ and $k^{(J,N)\leftarrow(J',N')}$, it is advisable to convert the master equation (10) into the integral form.

In order to determine the rate constants $k^{(J,N)\rightarrow(J',N')}$ and $k^{(J,N)\leftarrow(J',N')}$ by fitting them to the experimental data [the time profiles of the (J',N') states, $P^{J,N}_{J',N'}(t)$] in the $t>t_0$ regime it is advisable to convert the master equation (10) into the integral form. The integrated form of Eq. (10) is more stable against the noise of the experimental data because the statistical noise of the population profiles of the (J',N') states is averaged out by integration over time t. Furthermore, on the left-hand side of Eq. (10) we have the time derivation of a profile which of course is very sensitive regarding the statistical noise of the experimental data. This situation is illustrated in Fig. 8 where the statistical noise of the experimental data on the profile $P^{J,N}_{J,N}(t)$ of a NH($X\,^3\Sigma^-,v=0,J,N$) state which has been prepared at time t_0 by a dump laser pulse is shown (middle part). Also the time derivative $dP^{J,N}_{J,N}(t)/dt$ (top) and the integration over t $B^{J,N}_{J,N}(t)$ (bottom) of that profile are shown. One can recognize that the differentiation amplifies the statistical noise and the integration reduces the statistical noise. The integration causes a purposely averaging of the noisy data. So, if we integrate Eq. (10) on both sides from t_0 to t we obtain

$$\int_{t_0}^{t}\frac{dP^{J,N}_{J,N}(t)}{dt}dt = [\mathrm{C}]\sum_{(J',N')\neq(J,N)}^{(J',N')_{\max}}\left(k^{(J,N)\leftarrow(J',N')}\int_{t_0}^{t}P^{J,N}_{J',N'}(t)dt - k^{(J,N)\rightarrow(J',N')}\int_{t_0}^{t}P^{J,N}_{J,N}(t)dt\right). \tag{13}$$

With the definitions

$$\int_{t_0}^{t}P^{J,N}_{J',N'}(t)dt=I^{J,N}_{J',N'}(t) \quad \text{and} \quad \int_{t_0}^{t}P^{J,N}_{J,N}(t)dt=I^{J,N}_{J,N}(t) \tag{14}$$

for the integrated profiles of the populations and

$$P^{J,N}_{J,N}(t)-P^{J,N}_{J,N}(t_0)=B^{J,N}_{J,N}(t) \tag{15}$$

for the integrated profile of the initially populated state we can rewrite Eq. (13):

$$B^{J,N}_{J,N}(t)=[\mathrm{C}]\sum_{(J',N')\neq(J,N)}^{(J',N')_{\max}}\left(k^{(J,N)\leftarrow(J',N')}I^{J,N}_{J',N'}(t)-k^{(J,N)\rightarrow(J',N')}I^{J,N}_{J,N}(t)\right). \tag{16}$$

The rate constant $k^{(J,N)\rightarrow(J',N')}$ and $k^{(J,N)\leftarrow(J',N')}$ for the reverse reaction obey the microscopic reversibility relation[107] which can be written as

$$k^{(J,N)\rightarrow(J',N')}=k^{(J,N)\leftarrow(J',N')}\frac{g_{J',N'}}{g_{J,N}}e^{(E_{J,N}-E_{J',N'})/kT}, \tag{17}$$

where $E_{J,N}$ and $E_{J',N'}$ are the energies of the two involved states (J,N) and (J',N'). Equation (17) represents the fact that for $t\gg t_0$ the state population passes over to a Boltzmann distribution.

If we define the reversibility factor to be

$$R_{J,N,J',N'}=\frac{g_{J',N'}}{g_{J,N}}e^{(E_{J,N}-E_{J',N'})/kT}, \tag{18}$$

then we can replace $k^{(J,N)\leftarrow(J',N')}$ in Eq. (16) and obtain

$$B^{J,N}_{J,N}(t)=[\mathrm{C}]\sum_{(J',N')\neq(J,N)}^{(J',N')_{\max}}k^{(J,N)\rightarrow(J',N')}\times\left(R_{J',N',J,N}I^{J,N}_{J',N'}(t)-I^{J,N}_{J,N}(t)\right). \tag{19}$$

This equation does not contain the rate constant for the reverse reaction any more. Introducing the shortcut

$$R_{J',N',J,N}I^{J,N}_{J',N'}(t)-I^{J,N}_{J,N}(t)=D^{J,N}_{J,N,J',N'}(t) \tag{20}$$

we finally write

$$B^{J,N}_{J,N}(t)=-\sum_{(J',N')\neq(J,N)}^{(J',N')}B^{J,N}_{J',N'}(t)=[\mathrm{C}]\sum_{(J',N')\neq(J,N)}^{(J',N')_{\max}}k^{(J,N)\rightarrow(J',N')}D^{J,N}_{J,N,J',N'}(t). \tag{21}$$

In order to fit the rate constants $k^{(J,N)\rightarrow(J',N')}$ and implicitly $k^{(J,N)\leftarrow(J',N')}$ to the experimental data $P^{J,N}_{J',N'}(t)$ in the $t>t_0$ regime where secondary collisions occur we use an iterative algorithm which works as follows.

1. Determination of start values

At first it is necessary to use some start values for the rate constants which later will be improved repetitively. We obtain these start values from Eq. (21) by

$$k^{(J,N)\rightarrow(J',N')}=\frac{-B^{J,N}_{J',N'}(t)}{[\mathrm{C}]D^{J,N}_{J,N,J',N'}(t)} \tag{22}$$

for each initially prepared state (J,N). In principle it is also possible to use Eq. (12) in the $t\approx t_0$ regime to obtain the start values, but expression (22) takes implicitly the reverse reaction into consideration and is therefore suitable for higher t in contrast to expression (12). For states that have not been prepared directly by a laser pulse of the dump laser but for which the start values of the rate constants of the reverse transition can be obtained with Eq. (22) we used the reversibility relation (17) to obtain the start values. The remaining start values of rate constants which cannot be obtained that way are estimated by setting them to the value of a transition for which similar values are expected.

2. Calculation of new values for the $B^{J,N}_{J',N'}(t)$

Now one has to recalculate the values for the $B^{J,N}_{J',N'}(t)$ with Eq. (16) for all prepared J,N with the use of the values of the rate constants $k^{(J,N)\rightarrow(J',N')}$ and $k^{(J,N)\leftarrow(J',N')}$. The recalculation leads to values $B^{J,N}_{J',N',\mathrm{cal}}(t)$ which differ from the old ones because they reflect the current values of the rate constants. Because of the fact that the current rate constants are not the optimal ones, the $B^{J,N}_{J',N',\mathrm{cal}}(t)$ are either overestimated or underestimated. For that reason one needs improved values of the rate constants.

3. Improvement of the rate constants $k(J,N)\rightarrow(J',N')$

In order to improve the values of the rate constants $k^{(J,N)\rightarrow(J',N')}$ we use the ratio of $B^{J,N}_{J',N'}(t)/B^{J,N}_{J',N',\mathrm{cal}}(t)$ which represents the degree of correction if one assumes that most of the population of the (J',N') states comes directly from the initial prepared state (J,N). Thus, the expression

$$k^{(J,N)\rightarrow(J',N')}_{\mathrm{new}}=k^{(J,N)\rightarrow(J',N')}\frac{B^{J,N}_{J',N'}(t)}{B^{J,N}_{J',N',\mathrm{cal}}(t)} \tag{23}$$

generates the new values for the rate constants for all prepared J,N.

4. Calculation of the least squares sum

To monitor the convergence of the rate constants and to have a stop criterion for the iteration the least squares sum of the difference between the $B^{J,N}_{J',N',\mathrm{cal}}(t)$ and $B^{J,N}_{J',N'}(t)$ has to be calculated as a sum over all initially prepared states (J,N):

$$Q(t)_{\mathrm{new}}=\sum_{(J,N)\neq(J',N')}\left(B^{J,N}_{J',N'}(t)-B^{J,N}_{J',N',\mathrm{cal}}(t)\right)^2. \tag{24}$$

$Q(t)$ is the value that has to be minimal.

5. Definition of the break off criterion

The iteration is continued until the change in the value of $Q(t)$, $\Delta Q(t)$, is negligible. Therefore we define a convergence limit Q_{limit}. If $\Delta Q(t)>Q_{\mathrm{limit}}$ we continue with (2) otherwise the fit has finished. The value Q_{limit} has to be chosen such that the iteration breaks off after convergence has been achieved. Typically 5–10 iterations are enough to achieve convergence.

In order to generate population profiles which can be integrated continuously all experimental population profiles

TABLE II. State-to-state rate constants in units of $10^{-11}\,\mathrm{cm}^3\,\mathrm{molecule}^{-1}\,\mathrm{s}^{-1}$, for collision induced transitions. The accuracy is $0.08\times10^{-11}\,\mathrm{cm}^3\,\mathrm{molecule}^{-1}\,\mathrm{s}^{-1}$. The ''*'' sign indicates initial levels which have been prepared in the experiment. All state-to-state rate constants with such an initial level are determined directly. The ''–'' sign indicates initial levels which have not been prepared in the experiment. All rate constants with such an initial level are determined indirectly. The last row contains the sum of all rate constants which originate from the considered level indicated with a ''*'' or a ''–'' sign.

	Initial $N=0$, F_1 rate constants		
N	F_1	F_2	F_3
0	–		
1	1.82	0.85	0.33
2	1.20	0.14	0.10
3	0.24	0.14	0.23
4	0.02	0.02	0.36
5	0.00	0.00	0.04
6	0.00	0.01	0.04
7	0.00	0.00	0.02
8	0.00	0.00	0.00
	$\Sigma k=5.56$		

TABLE III. State-to-state rate constants in units of $10^{-11}\,\mathrm{cm}^3\,\mathrm{molecule}^{-1}\,\mathrm{s}^{-1}$, for collision induced transitions. The accuracy is $0.08\times10^{-11}\,\mathrm{cm}^3\,\mathrm{molecule}^{-1}\,\mathrm{s}^{-1}$. The ''*'' sign indicates initial levels which have been prepared in the experiment. All state-to-state rate constants with such an initial level are determined directly. The ''–'' sign indicates initial levels which have not been prepared in the experiment. All rate constants with such an initial level are determined indirectly. The last row contains the sum of all rate constants which originate from the considered level indicated with a ''*'' or a ''–'' sign.

	Initial $N=1$ rate constants								
	Initial $N=1$, F_1			Initial $N=1$, F_2			Initial $N=1$, F_3		
N	F_1	F_2	F_3	F_1	F_2	F_3	F_1	F_2	F_3
0	1.27			1.00			1.16		
1	*	3.05	4.37	4.29	*	1.16	2.17	3.45	–
2	1.86	0.24	0.20	0.87	1.22	0.75	2.26	1.59	1.13
3	1.57	0.28	0.05	0.61	1.29	0.16	2.36	0.66	0.90
4	0.08	0.28	0.01	0.02	0.35	0.02	0.05	0.70	0.51
5	0.00	0.02	0.02	0.00	0.02	0.01	0.00	0.25	0.12
6	0.02	0.21	0.18	0.00	0.00	0.00	0.00	0.98	0.08
7	0.23	0.00	0.01	0.01	0.00	0.02	0.00	0.42	0.02
8	0.00	0.00	0.01	0.01	0.03	0.00	0.00	0.00	0.00
	$\Sigma k=13.96$			$\Sigma k=11.84$			$\Sigma k=18.81$		

are modeled with smoothing spline functions. All integrals are calculated using the Romberg integration method. The calculations are realized in a *C* program.

IV. RESULTS AND DISCUSSION

Generally, we find a propensity for transitions to the neighboring quantum states. In these transitions either the nuclear rotation quantum number N is changed by ±1 or the index of the spin component i is changed by ±1. Transitions which change the nuclear rotation quantum number N or the index of the spin component i by more than ±1 are not effective. For transitions which change the nuclear rotation quantum number we find that transitions which increase the nuclear rotation quantum number N by 1 are more effective than transitions which decrease it by 1. Transitions which occur between high J states are less effective than transitions between low J states.

The complete set of state-to-state rate constants determined in this experiment is presented in Tables II–IX. For better clearness the (J,N) states are denoted as (N,F_i) states where $i=N+2-J$. The initially prepared (N,F_i) states are marked by ''*'' and the rate constants for collision induced transitions into all other states are determined directly by fitting them in the master equation. States which are indicated by a ''–'' sign represent initial states which have not been prepared in the experiment. In this case the rate constants for the collision induced transitions to all other states are calculated indirectly as described previously. The accuracy of the values was determined to be $0.08\times10^{-11}\,\mathrm{cm}^3\,\mathrm{molecule}^{-1}\,\mathrm{s}^{-1}$ by a linear fit in the $t\approx t_0$ regime using Eq. (12). The values for $\mathrm{NH}(X\,^3\Sigma^-,v=0,J=3,N=3)$ differ from our previously published values[84] because in this work a more accurate data analysis which includes the effect of multiple collisions is performed.

In the last row of each table the total rate constant for collision induced transitions out of the initial level is listed (the decrease of the initially prepared state), which represents the sum over all other rate constants. Figure 9 represents a plot of these total rate constants for the F_1, F_2, and F_3 levels as initial levels dependent on the initial nuclear rotation quantum number N. Also shown are the means of the total rate constants for F_1, F_2, F_3 states as initial states, i.e., the mean total rate constants. One recognizes that, apart from the variations, the total rate constant decreases with increasing N. This can be seen very clearly for the mean total rate constants. But also if the total rate constants are separated into F_1, F_2, and F_3 levels as initial levels this trend is visible. The total rate constants with F_1 levels as initial levels have the strongest decrease with N if we look at the slope, $\Delta(\Sigma k)/\Delta N$, of a linear regression fit $(\Delta(\Sigma k)/\Delta N=-1.63)$ followed by the rate constants with

TABLE IV. State-to-state rate constants in units of $10^{-11}\,\mathrm{cm}^3\,\mathrm{molecule}^{-1}\,\mathrm{s}^{-1}$, for collision induced transitions. The accuracy is $0.08\times10^{-11}\,\mathrm{cm}^3\,\mathrm{molecule}^{-1}\,\mathrm{s}^{-1}$. The ''*'' sign indicates initial levels which have been prepared in the experiment. All state-to-state rate constants with such an initial level are determined directly. The ''–'' sign indicates initial levels which have not been prepared in the experiment. All rate constants with such an initial level are determined indirectly. The last row contains the sum of all rate constants which originate from the considered level indicated with a ''*'' or a ''–'' sign.

	Initial $N=2$ rate constants								
	Initial $N=2$, F_1			Initial $N=2$, F_2			Initial $N=2$, F_3		
N	F_1	F_2	F_3	F_1	F_2	F_3	F_1	F_2	F_3
0	0.82			0.14			0.17		
1	1.62	0.27	0.44	0.40	1.54	0.44	0.44	1.02	0.52
2	*	4.34	0.17	6.18	*	2.39	0.41	3.96	–
3	2.82	0.80	0.15	0.36	1.44	0.66	0.10	0.32	0.35
4	0.17	0.29	0.73	0.23	0.07	0.00	0.20	0.01	0.32
5	0.05	0.02	0.42	0.16	0.00	0.00	0.00	0.01	0.01
6	0.26	0.03	0.01	0.00	0.00	0.00	0.00	0.00	0.31
7	0.10	0.01	0.03	0.00	0.00	0.04	0.00	0.00	0.00
8	0.01	0.01	0.01	0.00	0.00	0.00	0.00	0.00	0.00
	$\Sigma k=13.58$			$\Sigma k=14.05$			$\Sigma k=8.15$		

TABLE V. State-to-state rate constants in units of $10^{-11}\ \mathrm{cm}^3\ \mathrm{molecule}^{-1}\ \mathrm{s}^{-1}$, for collision induced transitions. The accuracy is $0.08\times 10^{-11}\ \mathrm{cm}^3\ \mathrm{molecule}^{-1}\ \mathrm{s}^{-1}$. The ‘‘*’’ sign indicates initial levels which have been prepared in the experiment. All state-to-state rate constants with such an initial level are determined directly. The ‘‘–’’ sign indicates initial levels which have not been prepared in the experiment. All rate constants with such an initial level are determined indirectly. The last row contains the sum of all rate constants which originate from the considered level indicated with a ‘‘*’’ or a ‘‘–’’ sign.

	Initial $N=3$ rate constants								
	Initial $N=3$, F_1			Initial $N=3$, F_2			Initial $N=3$, F_3		
N	F_1	F_2	F_3	F_1	F_2	F_3	F_1	F_2	F_3
0	0.21			0.16			0.36		
1	0.29	0.34	0.58	0.25	0.19	0.21	0.41	0.42	0.40
2	3.04	0.30	0.05	0.67	1.23	0.22	1.50	1.06	0.34
3	*	3.46	0.17	3.10	*	2.00	0.36	4.13	*
4	1.86	0.43	0.25	0.31	0.89	1.02	0.42	0.41	0.87
5	0.09	0.05	0.00	0.03	0.30	0.16	0.41	0.09	0.24
6	0.36	0.26	0.00	0.02	0.02	0.00	0.02	0.02	0.01
7	0.20	0.00	0.28	0.06	0.00	0.09	0.00	0.04	0.02
8	0.09	0.35	0.00	0.01	0.01	0.00	0.04	0.01	0.00
	$\Sigma k=12.66$			$\Sigma k=10.95$			$\Sigma k=11.58$		

TABLE VII. State-to-state rate constants in units of $10^{-11}\ \mathrm{cm}^3\ \mathrm{molecule}^{-1}\ \mathrm{s}^{-1}$, for collision induced transitions. The accuracy is $0.08\times 10^{-11}\ \mathrm{cm}^3\ \mathrm{molecule}^{-1}\ \mathrm{s}^{-1}$. The ‘‘*’’ sign indicates initial levels which have been prepared in the experiment. All state-to-state rate constants with such an initial level are determined directly. The ‘‘–’’ sign indicates initial levels which have not been prepared in the experiment. All rate constants with such an initial level are determined indirectly. The last row contains the sum of all rate constants which originate from the considered level indicated with a ‘‘*’’ or a ‘‘–’’ sign.

	Initial $N=5$ rate constants								
	Initial $N=5$, F_1			Initial $N=5$, F_2			Initial $N=5$, F_3		
N	F_1	F_2	F_3	F_1	F_2	F_3	F_1	F_2	F_3
0	0.00			0.01			0.15		
1	0.00	0.00	0.00	0.10	0.13	0.02	0.04	0.04	0.12
2	0.00	0.00	0.00	0.15	0.09	0.01	0.15	0.03	0.03
3	0.24	0.08	0.64	0.33	0.57	0.07	0.07	0.10	0.44
4	2.97	0.19	0.33	0.26	1.53	0.19	0.07	0.18	1.22
5	–	1.29	0.00	1.53	*	3.63	0.00	2.60	*
6	0.85	0.11	0.07	1.07	1.08	0.28	0.02	0.15	0.90
7	0.38	0.00	0.00	0.03	0.52	0.02	0.03	0.00	0.03
8	0.00	0.00	0.00	0.00	0.01	0.07	0.01	0.00	0.03
	$\Sigma k=7.15$			$\Sigma k=11.7$			$\Sigma k=6.41$		

F_3 ($\Delta(\Sigma k)/\Delta N=-1.34$) and F_2 ($\Delta(\Sigma k)/\Delta N=-0.47$) levels as initial level. Here the total rate constant for the ($N=0,F_1$) level as initial level is not taken into consideration because the situation for this rate constant is different. The value of this constant is essential lower because of the fact that the ($N=0,F_2$) state for which the strongest transition probability would be expected does not exist. The reason for the decrease of the total rate constants with increasing N is the increase of the energy spacing between the neighboring rotational levels and the typical strong dependence of the transferred energy in a collision.[108]

The mean total rate constant for transitions with F_1 levels as initial levels is $k_{F_1\rightarrow X}=9.76$, that for F_2 levels as initial levels is $k_{F_2\rightarrow X}=11.14$ and that for F_3 levels as initial levels is $k_{F_3\rightarrow X}=10.8$ [also here the total rate constant with the ($N=0,F_1$) level as initial level is not taken into consideration]. The mean rate constant for F_2 levels as initial levels is the strongest. The reason for this, as we see later, is the fact that in most cases the collision induced transitions which change the spin component by ±1 are the most effective collisions. But only transitions which originate from a F_2 level have two possibilities for such a transition. Transitions which originate from a F_1 level or a F_3 level have only one possibility for such a transition.

If we look at the single state-to-state rate constants (Tables II–IX) we realize that the largest values that can be

TABLE VI. State-to-state rate constants in units of $10^{-11}\ \mathrm{cm}^3\ \mathrm{molecule}^{-1}\ \mathrm{s}^{-1}$, for collision induced transitions. The accuracy is $0.08\times 10^{-11}\ \mathrm{cm}^3\ \mathrm{molecule}^{-1}\ \mathrm{s}^{-1}$. The ‘‘*’’ sign indicates initial levels which have been prepared in the experiment. All state-to-state rate constants with such an initial level are determined directly. The ‘‘–’’ sign indicates initial levels which have not been prepared in the experiment. All rate constants with such an initial level are determined indirectly. The last row contains the sum of all rate constants which originate from the considered level indicated with a ‘‘*’’ or a ‘‘–’’ sign.

	Initial $N=4$ rate constants								
	Initial $N=4$, F_1			Initial $N=4$, F_2			Initial $N=4$, F_3		
N	F_1	F_2	F_3	F_1	F_2	F_3	F_1	F_2	F_3
0	0.03			0.04			0.74		
1	0.29	0.12	0.02	0.24	0.09	0.32	0.27	0.20	0.30
2	0.81	0.24	0.16	0.52	0.20	0.01	0.28	0.28	0.42
3	1.98	0.28	0.15	0.51	1.17	0.11	1.34	1.51	1.23
4	*	1.77	0.17	1.39	*	2.75	0.21	4.32	*
5	1.61	1.16	0.08	0.12	1.10	0.25	0.28	0.21	0.67
6	0.04	0.02	0.01	0.02	0.00	0.07	0.46	0.02	0.08
7	0.02	0.00	0.01	0.13	0.00	0.02	0.02	0.00	0.10
8	0.09	0.00	0.01	0.01	0.00	0.00	0.01	0.00	0.00
	$\Sigma k=9.07$			$\Sigma k=9.07$			$\Sigma k=12.95$		

TABLE VIII. State-to-state rate constants in units of $10^{-11}\ \mathrm{cm}^3\ \mathrm{molecule}^{-1}\ \mathrm{s}^{-1}$, for collision induced transitions. The accuracy is $0.08\times 10^{-11}\ \mathrm{cm}^3\ \mathrm{molecule}^{-1}\ \mathrm{s}^{-1}$. The ‘‘*’’ sign indicates initial levels which have been prepared in the experiment. All state-to-state rate constants with such an initial level are determined directly. The ‘‘–’’ sign indicates initial levels which have not been prepared in the experiment. All rate constants with such an initial level are determined indirectly. The last row contains the sum of all rate constants which originate from the considered level indicated with a ‘‘*’’ or a ‘‘–’’ sign.

	Initial $N=6$ rate constants								
	Initial $N=6$, F_1			Initial $N=6$, F_2			Initial $N=6$, F_3		
N	F_1	F_2	F_3	F_1	F_2	F_3	F_1	F_2	F_3
0	0.00			0.03			0.03		
1	0.00	0.00	0.00	0.02	0.03	0.17	0.00	0.02	0.17
2	0.00	0.00	0.00	0.21	0.00	0.00	0.00	0.00	1.39
3	0.00	0.00	0.00	0.07	0.08	0.04	0.02	0.10	1.58
4	0.14	0.06	1.20	0.16	0.78	0.08	0.06	0.14	1.61
5	1.87	1.98	0.04	0.27	1.73	0.42	0.21	0.64	1.78
6	–	0.99	0.05	1.15	*	4.57	0.06	3.79	*
7	0.27	0.10	0.00	0.41	0.27	0.72	0.01	0.01	1.06
8	0.00	0.00	0.00	0.00	0.00	0.00	0.03	0.00	0.00
	$\Sigma k=6.7$			$\Sigma k=11.21$			$\Sigma k=12.71$		

TABLE IX. State-to-state rate constants in units of 10^{-11} cm^3 molecule^{-1} s^{-1}, for collision induced transitions. The accuracy is 0.08×10^{-11} cm^3 molecule^{-1} s^{-1}. The ''*'' sign indicates initial levels which have been prepared in the experiment. All state-to-state rate constants with such an initial level are determined directly. The ''–'' sign indicates initial levels which have not been prepared in the experiment. All rate constants with such an initial level are determined indirectly. The last row contains the sum of all rate constants which originate from the considered level indicated with a ''*'' or a ''–'' sign.

	Initial $N=7$ rate constants								
	Initial $N=7$, F_1			Initial $N=7$, F_2			Initial $N=7$, F_3		
N	F_1	F_2	F_3	F_1	F_2	F_3	F_1	F_2	F_3
0	0.00			0.00			0.04		
1	0.00	0.00	0.00	0.03	0.01	0.19	0.00	0.00	0.13
2	0.00	0.00	0.00	0.14	0.00	0.03	0.01	0.67	0.04
3	0.00	0.00	0.00	0.01	0.04	0.00	0.07	0.02	0.01
4	0.00	0.00	0.00	0.01	0.03	0.02	0.02	0.01	0.04
5	2.19	0.15	0.11	0.00	0.05	0.04	0.00	0.15	0.11
6	0.70	0.93	0.02	0.29	1.68	0.57	0.01	0.08	1.31
7	–	1.07	0.02	1.22	*	3.41	0.03	1.41	*
8	0.00	0.00	0.00	0.35	0.22	0.79	0.00	0.06	0.75
	$\Sigma k=5.19$			$\Sigma k=9.13$			$\Sigma k=4.97$		

found are between neighboring levels. These are the rate constants where the nuclear angular momentum does not change and the spin component F_i changes with a value of $\Delta i=\pm1$. If the spin component changes with a value of $\Delta i=\pm2$ the rate constant is much lower. For collision induced transitions which occur within the same spin component we observe a regular behavior like it is found in many other experiments described in the literature.[109] The transitions between neighboring levels have the largest values. Thus we find the following ''propensities''

$$\Delta N=0, \quad \Delta i=\pm1, \tag{25}$$

$$\Delta N=\pm1, \quad \Delta i=0. \tag{26}$$

Figure 10 represents a plot of the collision induced state-to-state rate constants for transitions between neighboring levels dependent on the initial N value. The initial levels in this case are the levels within the F_1 spin component. The general trend that the transition efficiency decreases with increasing N holds what supports the strong transition efficiency dependence on ΔE. For the same reason the transitions $(F_1\rightarrow F_1, N\rightarrow N-1)$ are more effective than the transitions $(F_1\rightarrow F_1, N\rightarrow N+1)$ except for $N<3$. For quantum numbers $N>3$ the transitions $(F_1\rightarrow F_1, N\rightarrow N-1)$ are the most effective transitions except for $N=7$ where $(F_1\rightarrow F_2, N\rightarrow N)$ transitions are slightly more effective. However, for low values of the quantum number N $(N<4)$ the transitions $(F_1\rightarrow F_2, N\rightarrow N)$ are most effective in energy transfer process except $N=1$ where the transition $(F_1\rightarrow F_3, N\rightarrow N)$ is the most effective one. For $N>1$ the $(F_1\rightarrow F_3, N\rightarrow N)$ energy transfer exhibits the lowest efficiency. It does not obey the propensity rules.

In principle, the same observations are made for F_2 (Fig. 11) and F_3 (Fig. 12). If we look at transitions which originate from the spin component F_2 (Fig. 11) we find that for low N values $(N<4)$ the transitions $(F_2\rightarrow F_1, N\rightarrow N)$ are the most effective ones. For $N>3$ the transitions $(F_2\rightarrow F_3, N\rightarrow N)$ are the most effective ones. The transitions $(F_2\rightarrow F_2, N\rightarrow N-1)$ and $(F_2\rightarrow F_2, N\rightarrow N+1)$ are less effective except for $N>5$. For these two transitions we find that the $\Delta N=+1$ transition is less effective than the $\Delta N=-1$ transition. For the transitions which have an F_3 level as the initial level (Fig. 12) we can clearly recognize that the transition with the highest efficiency is the transition $(F_3$

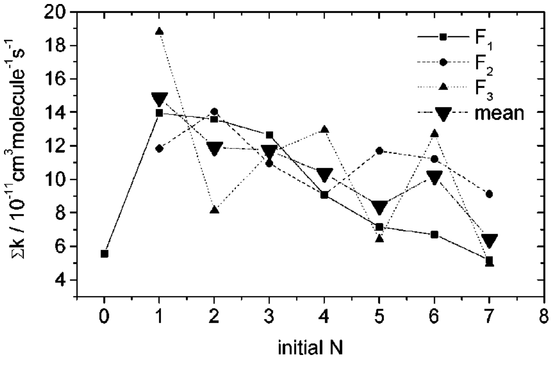

FIG. 9. Plot of the sum over all rate constants out of the (N,F_1), (N,F_2), and (N,F_3) states depending on the initial nuclear rotation quantum number N.

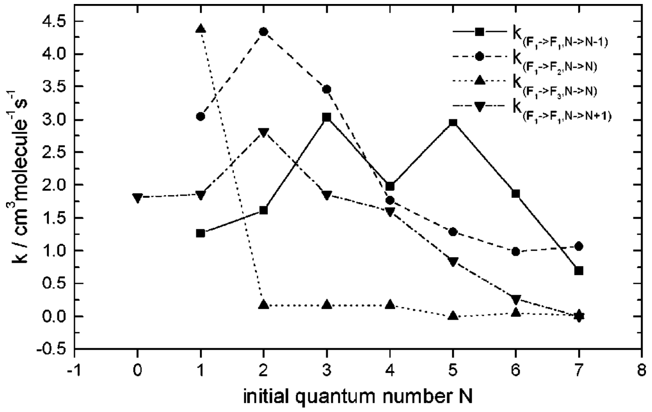

FIG. 10. State-to-state rate constants of collision induced transitions with a F_1 level as the initial level and a neighboring level as the final level depending on the initial nuclear rotation quantum number N.

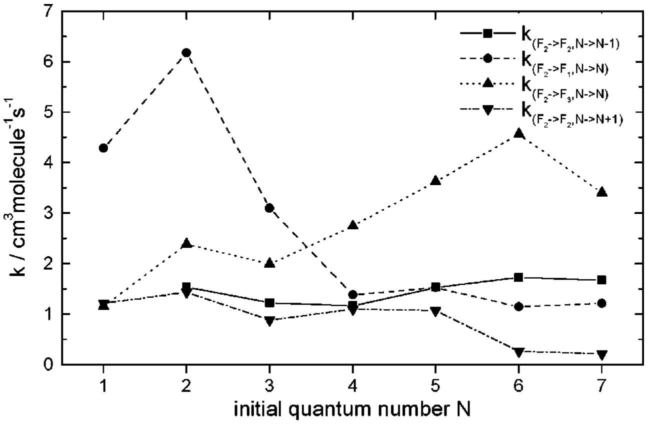

FIG. 11. State-to-state rate constants of collision induced transitions with a F_2 level as the initial level and a neighboring level as the final level depending on the initial nuclear rotation quantum number N.

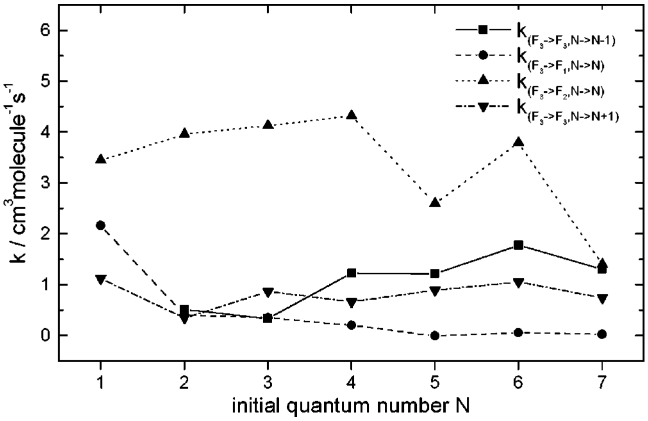

FIG. 12. State-to-state rate constants of collision induced transitions with a F_3 level as the initial level and a neighboring level as the final level depending on the initial nuclear rotation quantum number *N*.

$\rightarrow F_2, N \rightarrow N$). This fact holds for all initial *N*. The transition with the lowest transition probability is the transition ($F_3 \rightarrow F_1, N \rightarrow N$) which does not obey the propensity rules. Finally, the transitions ($F_3 \rightarrow F_3, N \rightarrow N-1$) are more effective than the transition ($F_3 \rightarrow F_3, N \rightarrow N+1$) except for $N=3$.

Previously, Dagdigian used a crossed beam apparatus to determine the relative cross sections for transitions out of the NH($X\,^3\Sigma^-, v=0, J=1, N=0$) state by collisions with argon at a collision energy of 410 cm^{-1}.[80] Because of the fact that argon is a structureless target this state-to-state cross sections should be qualitatively comparable to the state-to-state rate constants we obtained. In fact the qualitative result is the same. Transitions to the ($N=1, F_1$) level are the most effective transitions. The efficiency decreases with increasing *N* and the efficiency of transitions into levels which change the spin component more than 1 unit are ineffective. The results of Dagdigian are therefore in agreement with our observations and support our propensity rules.

Table X represents the state-to-state rate constants that result if only the nuclear rotation quantum number *N* is considered. The values are obtained by calculating the mean value concerning the three initial states (N, F_1), (N, F_2), and (N, F_3) and calculating the sum over the three final states (N', F_1), (N', F_2), (N', F_3). One recognizes a strong dependency on the change of the nuclear rotation quantum number *N*. This again implies a strong dependency on the amount of the transferred energy ΔE. In order to quantify the dependency on the value of the transferred energy, ΔE, we use a special two parameter version (for vibrationally elastic collisions)[110] of the well-known scaling law, called the energy-gap law (EGL). The inelastic state-to-state collision rate constant can therefore be expressed by

$$k_{N \rightarrow N'}^{\mathrm{EGL}} = a(2N'+1)e^{(\beta \Delta E/kT)} \tag{27}$$

with $\Delta E = |E_{N'} - E_N|$. We divide both sides by the standard rate constant $k_0 = 10^{-11}\,\mathrm{cm}^{-3}\,\mathrm{molecule}^{-1}\,\mathrm{s}^{-1}$. Now we can write

$$\ln\left(\frac{k_{N \rightarrow N'}^{\mathrm{EGL}}}{k_0(2N'+1)}\right) = \ln\left(\frac{a}{k_0}\right) - \beta\left(\frac{\Delta E}{kT}\right) \tag{28}$$

in order to perform a linear fit to our experimental data. The results of the fit are listed in Table XI which also contains the fit results for separately fitting the data for every single initial quantum number *N*. A plot of the linear fit is presented in Fig. 13. One recognizes that the general shape of the experimentally determined values obeys this linear representation of the rate constants dependent from the transferred energy in an inelastic collision. In order to examine the detailed energy dependence for every single initial quantum number *N* we performed these linear fits for every single initial quantum number *N*. Figure 14 shows the plots of the linear fits for separate initial *N*. One can recognize that in spite of the fact that the fitting parameters *a* and β vary the linear behavior holds for every single fit.

TABLE X. State-to-state rate constants in units of $10^{-11}\,\mathrm{cm}^3\,\mathrm{molecule}^{-1}\,\mathrm{s}^{1}$, for collision induced transitions only considering the nuclear rotation quantum number *N*.

Final state *N*	Initial quantum state *N*							
	0	1	2	3	4	5	6	7
0	–	1.14	0.38	0.24	0.27	0.05	0.02	0.01
1	3.00	–	2.23	1.04	0.62	0.16	0.14	0.12
2	1.44	3.37	–	2.80	0.98	0.06	0.53	0.29
3	0.61	2.62	2.33	–	2.77	0.84	0.63	0.05
4	0.40	0.76	0.67	2.15	–	2.31	1.41	0.04
5	0.04	0.15	0.22	0.46	1.82	–	2.98	0.94
6	0.05	0.14	0.21	0.70	0.23	1.52	–	1.86
7	0.02	0.24	0.05	0.23	0.10	0.34	0.95	–
8	0.00	0.01	0.00	0.17	0.04	0.03	0.01	0.72

TABLE XI. Energy-gap law (EGL) parameters for collision induced transitions between different *N* states. *a* in units of $10^{-11}\,\mathrm{cm}^3\,\mathrm{molecule}^{-1}\,\mathrm{s}^{-1}$. β is dimensionless.

Initial *N*	0–7	0	1	2	3	4	5	6	7
a	0.5	0.53	0.80	0.62	0.48	0.95	1.49	0.32	0.11
Δa	0.1	0.3	0.4	0.2	0.2	0.5	0.5	0.2	0.1
β	1.13	1.54	1.27	1.41	0.92	1.56	0.45	0.62	0.46
$\Delta\beta$	0.1	0.2	0.2	0.2	0.1	0.3	0.1	0.3	0.3

V. CONCLUSION

We examined the state-to-state rotational energy transfer of the collision system NH($X\,^3\Sigma^-, v=0, J, N$)+Ne. A new preparation technique for the state selective preparation of the ground state NH($X\,^3\Sigma^-, v=0, J, N$) radicals[84] is used. This technique is based on two steps. In the first step a strong population inversion between the NH($X\,^3\Sigma^-$) ground state and the metastable excited NH($a\,^1\Delta$) state ($\tau \approx 12.5$ s) is generated by the photolysis of HN_3 at a wavelength of 266 nm where no NH($X\,^3\Sigma^-$) ground state radicals are produced. In the second step NH($X\,^3\Sigma^-, v=0, J, N$) radicals are prepared state-selectively via stimulating the strongly forbidden NH($a\,^1\Delta, v=0 \rightarrow X\,^3\Sigma^-, v=0$) intercombination transition around 794 nm. The initially state-selectively prepared NH($X\,^3\Sigma^-, v=0, J, N$) radicals are detected with laser induced fluorescence (LIF) in a third step after certain delay times and at certain total pressures in the observation chamber when first collisions have occurred. With this technique

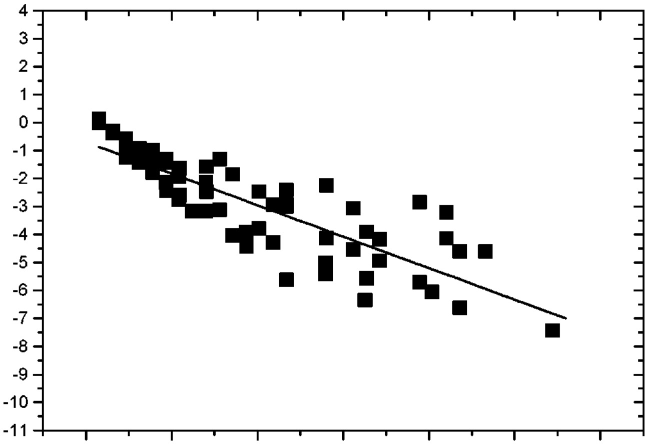

FIG. 13. Logarithmic energy-gap law (EGL) plot of ($N\rightarrow 0,1,...,8$) transitions. The straight line represents the linear fit that results in the obtained EGL constants. The plot shows that the energy-gap law describes the gross dependence of rate constants from the transferred energy.

it was possible to examine state-to-state energy transfer in ground state NH($X\,{}^3\Sigma^-,v=0,J,N$) for higher N levels than $N=0,1$ for the first time.

Series of LIF spectra were recorded and fitted in order to determine the population distributions at different collision numbers. The population data were modeled using smoothing spline functions and state-to-state rate constants were calculated by iterative algorithm that integrates the population profiles.

The calculated rate constants imply the propensity rules

$$\Delta N=0,\quad \Delta i=\pm 1\quad \text{and}\ \Delta N=\pm 1,\quad \Delta i=0.$$

In most of the cases the transitions which change the spin component by a value of ±1 and conserve the nuclear rotation quantum number N are the most effective collisions.

The obtained rate constants qualitatively agree with those obtained in a crossed beam experiment for the lowest rotational level.

The ($N\rightarrow N'$) rate constants, which represent the rate constants that are obtained if only the change in the nuclear rotation quantum number is considered, were extracted from the state-to-state rate constants by calculating the mean value concerning the three initial spin components and calculating the sum over the three final spin components. The detailed dependence of the ($N\rightarrow N'$) rate constants from the transferred energy is examined by fitting the experimental data to

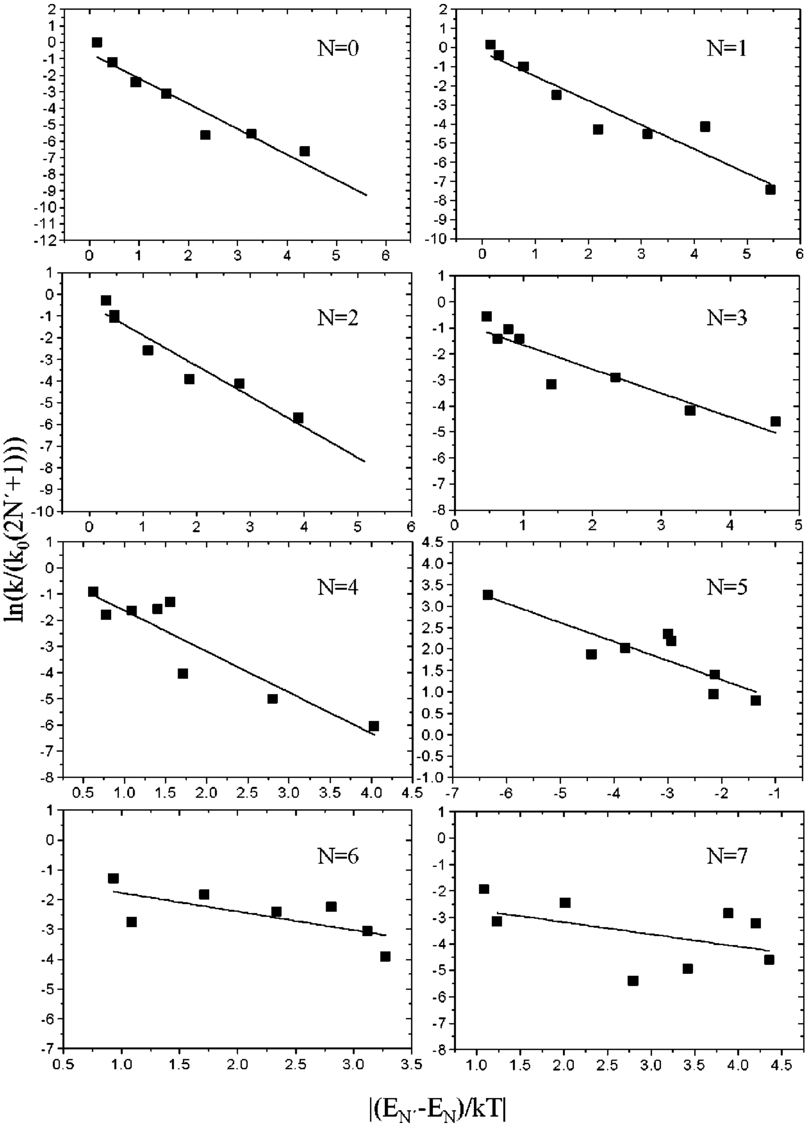

FIG. 14. Logarithmic energy-gap law (EGL) plots of ($N\rightarrow 0,1,...,8$) transitions separated for different initial N.

a special two parameter energy-gap law (EGL) for vibrationally elastic collisions.[110] EGL parameters for every single initial quantum number N are calculated. In spite of the fact that the EGL parameters are different for every initial quantum number N and that the resolved state-to-state rate constants $(J,N \rightarrow J'N')$ from which the $(N \rightarrow N')$ rate constants are calculated vary tremendously, the EGL is found to describe the values of the rate constants which means that the behavior of the rate constants concerning the transferred energy and implicitly the quantum number N is found to be regular.

ACKNOWLEDGMENT

Support of this work by the Deutsche Forschungsgemeinschaft and Fonds der Chemischen Industrie is gratefully acknowledged.

[1] M. J. Reid and J. M. Moran, Annu. Rev. Astron. Astrophys. **19**, 231 (1981).
[2] M. Elitzur, Rev. Mod. Phys. **54**, 1225 (1982).
[3] P. Andresen, N. Aristov, V. Beushausen, D. Häusler, and H. W. Lülf, J. Chem. Phys. **95**, 5763 (1991).
[4] M. M. Litvak and E. N. Rodriquez Kuiper, Astrophys. J. **253**, 622 (1982).
[5] D. L. Lambert, J. A. Brown, K. A. Hinkle, and H. R. Johnson, Astrophys. J. **284**, 223 (1984).
[6] I. Glassman, *Combustion* (Academic, New York, 1977), p. 219.
[7] G. B. Debrou, J. M. Goodings, and D. K. Bohme, Combust. Flame **39**, 1 (1980).
[8] J. Franck and R. W. Wood, Philos. Mag. **21**, 314 (1911).
[9] R. B. Kurzel, J. I. Steinfeld, D. A. Hatzenbuhler, and G. E. Leroi, J. Chem. Phys. **55**, 4822 (1971).
[10] S. L. Dexheimer, M. Durand, T. A. Brunner, and D. E. Pritchard, J. Chem. Phys. **76**, 4996 (1982).
[11] H. Chun, H. Ruiping, and Z. Cunhao, Appl. Phys. B: Photophys. Laser Chem. **41**, 251 (1986).
[12] R. K. Lengel and D. R. Crosley, J. Chem. Phys. **67**, 2085 (1977).
[13] K. Bergmann and W. Demtröder, Z. Phys. **243**, 1 (1971).
[14] T. A. Brunner, R. D. Driver, N. Smith, and D. E. Pritchard, Phys. Rev. Lett. **41**, 856 (1978).
[15] M. Wainger *et al.*, J. Chem. Phys. **71**, 1977 (1979).
[16] T. A. Brunner, R. D. Driver, N. Smith, and D. E. Pritchard, J. Chem. Phys. **70**, 4155 (1979).
[17] T. Brunner, N. Smith, and D. E. Pritchard, Chem. Phys. Lett. **71**, 358 (1980).
[18] T. A. Brunner, N. Smith, A. W. Karp, and D. E. Pritchard, J. Chem. Phys. **74**, 3324 (1981).
[19] Ch. Ottinger and M. Schröder, J. Phys. B **13**, 4163 (1980).
[20] T. P. Scott, N. Smith, and D. E. Pritchard, J. Chem. Phys. **80**, 4841 (1984).
[21] J. Dufayard and O. Nédélec, Chem. Phys. **71**, 279 (1982).
[22] O. Nédélec and J. Dufayard, Chem. Phys. **105**, 371 (1986).
[23] M. Giroud and O. Nédélec, J. Chem. Phys. **77**, 3998 (1982).
[24] O. Nédélec and J. Dufayard, Chem. Phys. **84**, 167 (1984).
[25] M. Ferray, J. P. Visticot, and B. Sayer, J. Chem. Phys. **81**, 3009 (1984).
[26] C. Dufour, B. Pinchemel, M. Douay, J. Schamps, and M. H. Alexander, Chem. Phys. **98**, 315 (1985).
[27] S. J. Davis and K. W. Holtzclaw, J. Chem. Phys. **92**, 1661 (1990).
[28] S. D. Augustin and W. H. Miller, J. Chem. Phys. **61**, 3155 (1974).
[29] S. Green, B. J. Carrison, W. A. Lester, Jr., and W. H. Miller, Astrophys. J., Suppl. Ser. **37**, 321 (1978).
[30] S. Green, J. Chem. Phys. **64**, 3463 (1976).
[31] S. Green, J. Chem. Phys. **70**, 816 (1979).
[32] S. Green, J. Chem. Phys. **73**, 2740 (1980).
[33] S. L. Davis and J. E. Boggs, J. Chem. Phys. **69**, 2355 (1978).
[34] S. L. Davis, J. Chem. Phys. **77**, 5856 (1982).
[35] S. L. Davis and S. Green, J. Chem. Phys. **78**, 2170 (1983).
[36] R. N. Dixon and D. Field, Proc. R. Soc. London, Ser. A **366**, 225 (1979).
[37] M. H. Alexander, J. Chem. Phys. **77**, 1855 (1982).
[38] B. J. Whitaker and A. J. McCaffery, J. Chem. Phys. **78**, 3857 (1983).
[39] D. Clary, J. Chem. Phys. **78**, 4915 (1983).
[40] H. Klar, J. Phys. B **6**, 2139 (1973).
[41] S. Green and R. N. Zare, Chem. Phys. **7**, 62 (1975).
[42] S. I. Chu, Astrophys. J. **206**, 6110 (1976).
[43] R. N. Dixon and D. Field, Proc. R. Soc. London, Ser. A **368**, 99 (1979).
[44] M. Shapiro and H. Kaplan, J. Chem. Phys. **71**, 2182 (1979).
[45] D. P. Dewangan and D. R. Flower, J. Phys. B **14**, 2179 (1982).
[46] M. H. Alexander, J. Chem. Phys. **76**, 3637,5974 (1982).
[47] S. L. Davis and M. H. Alexander, J. Chem. Phys. **78**, 800 (1983).
[48] M. H. Alexander and P. J. Dagdigian, J. Chem. Phys. **79**, 302 (1983).
[49] J. J. Hinchen, Appl. Phys. Lett. **27**, 672 (1975).
[50] J. J. Hinchen and R. H. Hobbs, J. Chem. Phys. **65**, 2732 (1976).
[51] R. A. Copeland, D. J. Pearson, and F. F. Crim, Chem. Phys. Lett. **81**, 541 (1981).
[52] R. A. Copeland and F. F. Crim, J. Chem. Phys. **78**, 5551 (1983).
[53] W. Meier, G. Ahlers, and H. Zacharias, J. Chem. Phys. **85**, 2599 (1986).
[54] R. L. Farrow and D. W. Chandler, J. Chem. Phys. **89**, 1994 (1988).
[55] J. Arnold, T. Dreier, and D. W. Chandler, Chem. Phys. **133**, 123 (1989).
[56] D. W. Chandler and R. L. Farrow, J. Chem. Phys. **85**, 810 (1986).
[57] F. Menard-Bourcin, T. Delaporte, and J. Menard, J. Chem. Phys. **84**, 201 (1986).
[58] E. A. Rohlfing, D. W. Chandler, and D. H. Parker, J. Chem. Phys. **87**, 5229 (1987).
[59] R. Fei *et al.*, J. Chem. Phys. **100**, 1190 (1994).
[60] A. Jörg, U. Meier, and K. Kohse-Höinghaus, J. Chem. Phys. **93**, 6453 (1990).
[61] J. L. Cooper and J. Whitehead, J. Phys. Chem. **98**, 8274 (1994).
[62] Ch. Ottinger, R. Valesco, and R. N. Zare, J. Chem. Phys. **52**, 1636 (1970).
[63] Ch. Ottinger, Chem. Phys. **1**, 161 (1973).
[64] Ch. Ottinger and D. Poppe, Chin. Phys. **8**, 513 (1971).
[65] D. Lemoine, G. C. Corey, M. H. Alexander, and J. Derouard, Chem. Phys. **118**, 357 (1987).
[66] K. Bergmann and W. Demtröder, J. Phys. B **5**, 1386 (1972).
[67] O. Nédélec and J. Dufayard, J. Chem. Phys. **76**, 378 (1982).
[68] P. J. Dagdigian, M. H. Alexander, and K. Liu, J. Chem. Phys. **91**, 839 (1989).
[69] M. H. Alexander and P. J. Dagdigian, J. Chem. Phys. **101**, 7468 (1994).
[70] M. H. Alexander, W. R. Kearney, and A. F. Wagner, J. Chem. Phys. **100**, 1338 (1994).
[71] P. Andresen, N. Aristov, V. Beushausen, D. Häusler, and H. W. Lülf, J. Chem. Phys. **95**, 5763 (1991).
[72] A. D. Esposti, A. Berning, and H.-J. Werner, J. Chem. Phys. **103**, 2067 (1995).
[73] G. C. Corey and M. H. Alexander, J. Chem. Phys. **88**, 6931 (1988).
[74] T. A. Caughey and D. R. Crosley, J. Chem. Phys. **69**, 3379 (1978).
[75] T. A. Caughey and D. R. Crosley, J. Chem. Phys. **71**, 736 (1979).
[76] R. N. Dixon, J. Chem. Soc., Faraday Trans. 2 **83**, 675 (1987).
[77] P. J. Dagdigian, J. Chem. Phys. **90**, 6110 (1989).
[78] K. Schreel, J. Schleipen, A. Eppink, and J. J. ter Meulen, J. Chem. Phys. **99**, 8713 (1993).
[79] J. A. Mack, K. Mikulecky, and A. M. Wodke, J. Chem. Phys. **105**, 4105 (1996), and Refs. 1–18 therein.
[80] P. J. Dagdigian, J. Chem. Phys. **90**, 6110 (1989).
[81] A. Kaes and F. Stuhl, J. Chem. Phys. **97**, 4661 (1992).
[82] M. Yang *et al.*, J. Chem. Phys. **102**, 4069 (1995).
[83] L. Neitsch, F. Stuhl, P. J. Dagdigian, and M. H. Alexander, J. Chem. Phys. **104**, 1325 (1996).
[84] J. L. Rinnenthal and K.-H. Gericke, J. Chem. Phys. **111**, 9465 (1999).
[85] J. R. McDonald, R. G. Miller, and A. P. Baronavski, Chem. Phys. Lett. **51**, 57 (1977).
[86] J. R. McDonald, R. G. Miller, and A. P. Baronavski, Chem. Phys. **30**, 133 (1978).
[87] H. H. Nelson and J. R. McDonald, J. Chem. Phys. **93**, 8777 (1990).
[88] M. Hawley, A. P. Baronavski, and H. H. Nelson, J. Chem. Phys. **99**, 2638 (1993).
[89] J. L. Rinnenthal and K.-H. Gericke, J. Mol. Spectrosc. **198**, 115 (1999).
[90] K.-H. Gericke, M. Lock, R. Fasold, and F. J. Comes, J. Chem. Phys. **96**, 422 (1992).
[91] M. Hawley, A. P. Baronavski, and H. H. Nelson, J. Chem. Phys. **99**, 2638 (1993).
[92] K.-H. Gericke, T. Haas, M. Lock, R. Theinl, and F. J. Comes, J. Phys. Chem. **95**, 6104 (1991).
[93] J. M. Eder, Denkschr. Wien. Akad. **60**, 1 (1893).

[94] G. W. Funke, Z. Phys. **96**, 787 (1935).
[95] R. N. Dixon, Can. J. Phys. **37**, 1171 (1959).
[96] J. Malicet, J. Brion, and H. Guenebaut, J. Chim. Phys. **67**, 25 (1970).
[97] C. R. Brazier, R. S. Ram, and P. F. Bernath, J. Mol. Spectrosc. **120**, 381 (1986).
[98] R. S. Ram, P. F. Bernath, and K. H. Hinkle, J. Chem. Phys. **110**, 5557 (1999).
[99] J. M. Brown *et al.*, J. Mol. Spectrosc. **55**, 500 (1975).
[100] B. Pouilly, P. J. Dagdigian, and M. H. Alexander, J. Chem. Phys. **87**, 7118 (1987).
[101] G. Herzberg, *Spectra of Diatomic Molecules*, 2nd ed. (Van Nostrand–Reinhold, New York, 1950).
[102] I. Kovacs, *Rotational Structure in the Spectra of Diatomic Molecules* (Hilger, London, 1969).
[103] A. Schadee, Astron. Astrophys. **41**, 203 (1975).
[104] A. Schadee, Astron. Astrophys. **41**, 213 (1975).
[105] P. Nolan and F. A. Jenkins, Phys. Rev. **50**, 943 (1963).
[106] P. W. Fairchild, G. P. Smith, D. R. Crosley, and J. B. Jeffries, Chem. Phys. Lett. **107**, 181 (1984).
[107] J. I. Steinfeld, J. S. Francisco, and W. L. Hase, *Chemical Kinetics and Dynamics* (Prentice-Hall, New Jersey, 1989).
[108] N. C. Lang, J. C. Polanyi, and J. Wanner, Chem. Phys. **24**, 219 (1977).
[109] R. D. Levine and R. B. Bernstein, *Molecular Reaction Dynamics and Chemical Reactivity* (Oxford University Press, New York, 1987).
[110] J. I. Steinfeld and P. Ruttenberg, Report No. 23, Atomic Collisions Data Center, Joint Institute for Laboratory Astrophysics, Boulder, CO, 1983.
[111] F. Freitag, F. Rohrer, and F. Stuhl, J. Phys. Chem. **93**, 3170 (1989).
[112] R. D. Bower, M. T. Jacoby, and J. A. Blauer, J. Chem. Phys. **86**, 1954 (1987).